Article
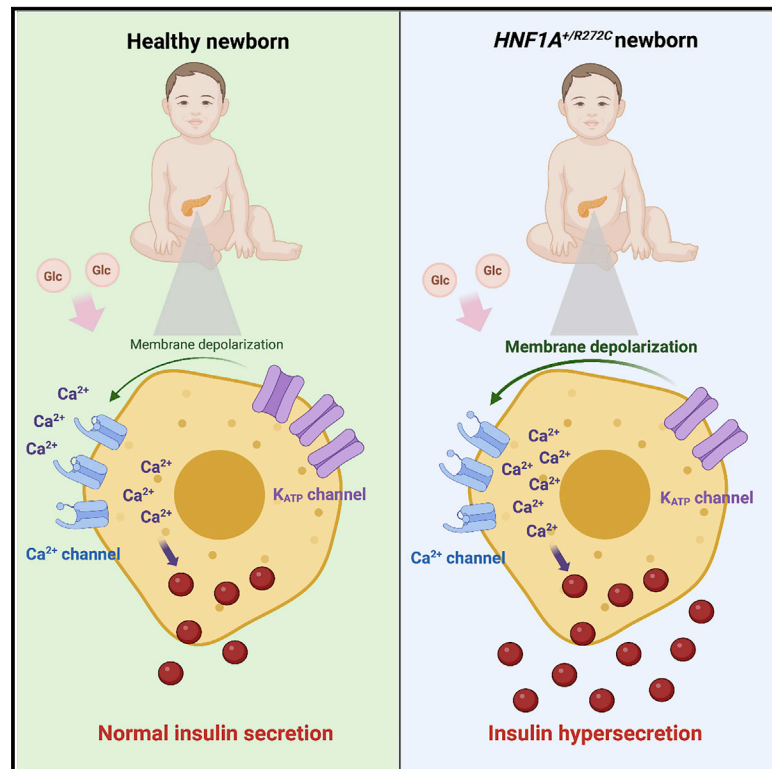
An insulin hypersecretion phenotype precedes pancreatic β cell failure in MODY3 patient-specific cells

Graphical abstract

Highlights

- *HNF1A$^{+/R272C}$* β cells exhibit the insulinotropic effect of SU used in the clinic

- *HNF1A$^{+/R272C}$* β cells hypersecrete insulin *in vitro* and *in vivo*

- Trend of increased birth weight in human *HNF1A$^{+/G292fs}$* carriers versus healthy siblings

- K$_{ATP}$ channel downregulation underlies insulin hypersecretion in *HNF1A$^{+/R272C}$* β cells

Authors

Florian M. Hermann,
Maya Friis Kjærgaard,
Chenglei Tian, ..., Tiinamaija Tuomi,
Ivana Novak, Henrik Semb

Correspondence

henrik.semb@helmholtz-muenchen.de

In brief

Hermann et al. used patient-derived stem cells to study why mutations in *HNF1A* progressively lead to diabetes in MODY3. The studied MODY3 mutation caused hypersecretion of insulin from β cells due to altered expression of ion channels. Their findings identify a new pathogenic mechanism for diabetes onset in MODY3.

CellPress

Article

An insulin hypersecretion phenotype precedes pancreatic β cell failure in MODY3 patient-specific cells

Florian M. Hermann,[1,11] Maya Friis Kjærgaard,[1,11] Chenglei Tian,[1,2] Ulf Tiemann,[1] Abigail Jackson,[1] Lars Rønn Olsen,[3] Maria Kraft,[4] Per-Ola Carlsson,[5,6] Iina M. Elfving,[7] Jarno L.T. Kettunen,[7,8,9] Tiinamaija Tuomi,[7,8,9] Ivana Novak,[10] and Henrik Semb[1,2,12,*]

[1]Novo Nordisk Foundation Center for Stem Cell Biology (DanStem), University of Copenhagen, Copenhagen, Denmark
[2]Institute of Translational Stem Cell Research, Helmholtz Diabetes Center, Helmholtz Zentrum München, München, Germany
[3]Department of Health Technology, Technical University of Denmark, Kongens Lyngby, Denmark
[4]Lund Stem Cell Center, Lund University, Lund, Sweden
[5]Department of Medical Cell Biology, Uppsala University, Uppsala, Sweden
[6]Department of Medical Sciences, Uppsala University, Uppsala, Sweden
[7]Folkhalsan Research Center, Helsinki, Finland
[8]Institute for Molecular Medicine Finland, University of Finland, Helsinki, Finland
[9]Department of Endocrinology, Abdominal Center, Helsinki University Hospital, Helsinki, Finland
[10]Department of Biology, University of Copenhagen, Copenhagen, Denmark
[11]These authors contributed equally
[12]Lead contact
*Correspondence: henrik.semb@helmholtz-muenchen.de
https://doi.org/10.1016/j.stem.2022.12.001

SUMMARY

MODY3 is a monogenic hereditary form of diabetes caused by mutations in the transcription factor *HNF1A*. The patients progressively develop hyperglycemia due to perturbed insulin secretion, but the pathogenesis is unknown. Using patient-specific hiPSCs, we recapitulate the insulin secretion sensitivity to the membrane depolarizing agent sulfonylurea commonly observed in MODY3 patients. Unexpectedly, MODY3 patient-specific $HNF1A^{+/R272C}$ β cells hypersecrete insulin both *in vitro* and *in vivo* after transplantation into mice. Consistently, we identified a trend of increased birth weight in human HNF1A mutation carriers compared with healthy siblings. Reduced expression of potassium channels, specifically the K_{ATP} channel, in MODY3 β cells, increased calcium signaling, and rescue of the insulin hypersecretion phenotype by pharmacological targeting ATP-sensitive potassium channels or low-voltage-activated calcium channels suggest that more efficient membrane depolarization underlies the hypersecretion of insulin in MODY3 β cells. Our findings identify a pathogenic mechanism leading to β cell failure in MODY3.

INTRODUCTION

Maturity-onset diabetes of the young (MODY) accounts for 1%–2% of diabetes cases, and MODY3 is typically the most common form of monogenic diabetes in Caucasian populations.[1] MODY3 is caused by heterozygous mutations in the transcription factor *HNF1A*. The main clinical symptoms are progressive hyperglycemia due to perturbed insulin (INS) secretion and glycosuria as a result of a lower renal glucose threshold.[2,3] Low doses of sulfonylureas (SUs) are often an effective first-line therapy for MODY3 patients, allowing good glycaemic control and reducing the risk of hypoglycemia compared with INS treatment.[4] Hence, the β cells of MODY3 patients are still able to produce and release INS. The main effect of SUs in β cells is considered to be the inhibition of ATP-sensitive potassium (K_{ATP}) channels, leading to a depolarization of the cell membrane, Ca^{2+} ion influx and consequential INS secretion.[5] Patients with other diabetes types, such as type 2 diabetes, are less sensitive to SUs,[6] which suggests that membrane potential could be affected in MODY3 patients.

The phenotype of MODY3 patients is very heterogeneous, which is reflected by, among other things, a highly variable age at disease onset.[7–9] Despite many efforts in trying to understand the underlying disease mechanism of MODY3, the determinants of disease onset are poorly understood.[10] A better understanding of what triggers diabetes in MODY3 patients would open up for targeted treatments that delay or even prevent the disease.

In murine *Hnf1a* homozygous knockout models, reduced glucose import and glycolytic flux have been proposed to be caused by a deregulation of the glucose transporter *Slc2a2* (also known as *Glut2*) and the glycolytic gene *Pklr*.[11–13] However,
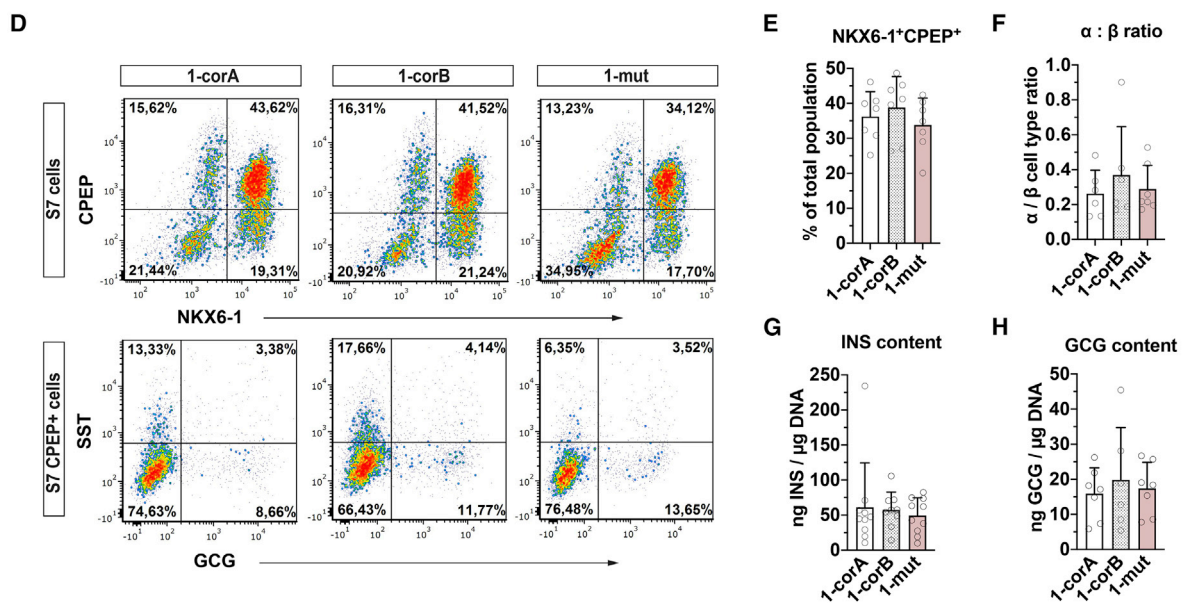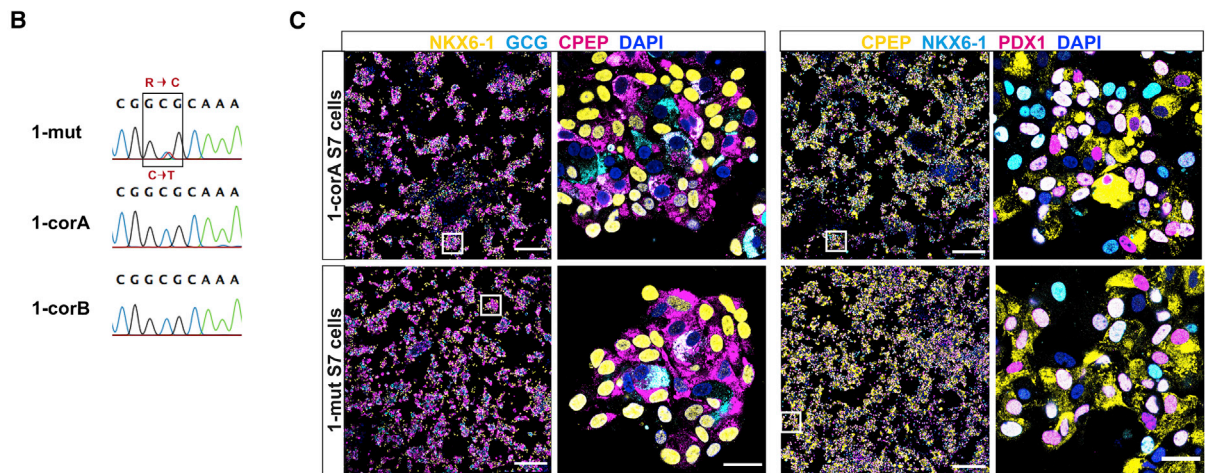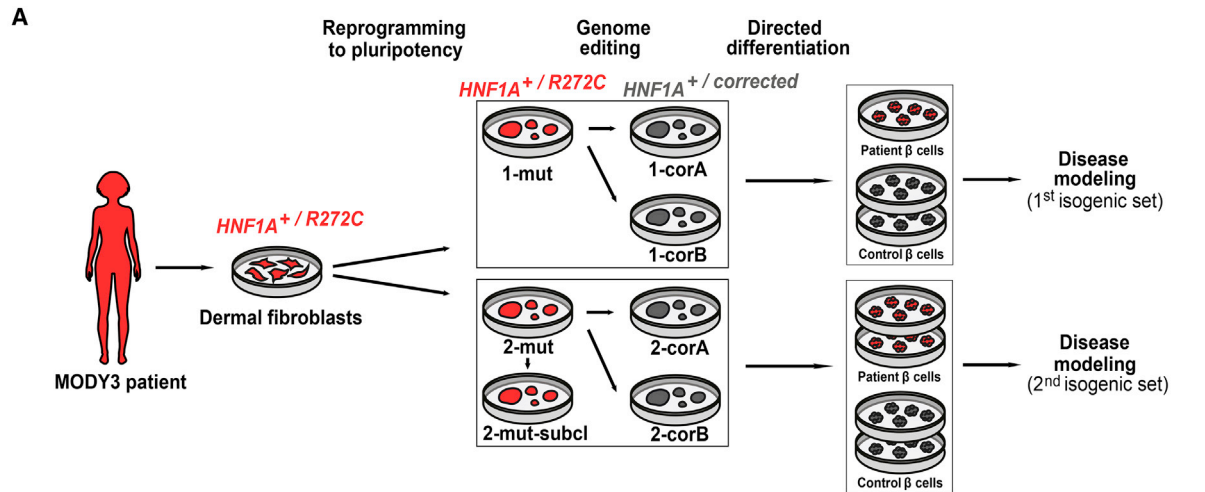
(legend on next page)

MODY3 is most likely caused by other mechanisms affecting endocrine function, since SLC2A2 is not the main glucose transporter in human β cells[14] and PKLR is not catalyzing a rate-limiting step in glycolysis.[15]

To model MODY3 in human β cells, human embryonic stem cell (hESC) lines with homozygous null mutations in *HNF1A*[16,17] or human induced pluripotent stem cells (hiPSCs) with patient-specific mutations in *HNF1A*[17–19] have recently been used. Both mutant hESC- and hiPSC-derived β cells displayed perturbed glucose stimulated INS secretion (GSIS), and the suggested mechanisms were impaired glycolysis and mitochondrial function,[16] reduced calcium levels and abnormal INS granules,[17] and impaired glucose uptake due to a downregulation of *SLC2A2*.[18] The progressive nature of the disease suggests that these studies primarily model various aspects of the pathophysiology of MODY3 and not the upstream mechanism. Cardenas-Diaz et al.[16] and González-lez et al.[17] also showed that *HNF1A*-deficient hESCs were characterized by a differentiation bias toward the α cell lineage that was proposed to be caused by reduced expression of the β cell determinant *PAX4*, whereas Cujba et al.[19] reported a compromised ability of hiPSCs with a *HNF1A*+/291fs mutation to differentiate into pancreatic endoderm and endocrine lineages.[19]

MODY3 patients are hyperresponsive to SUs compared with other diabetic patients and SUs more efficiently stimulate INS secretion in MODY3 patients than GLP1 analogs.[6,20] To capture these patient characteristics, we generated MODY3 patient-specific hiPSC lines which successfully recapitulated the sensitivity to SUs compared with isogenic corrected control hiPSC lines. We set out to investigate potential disease mechanisms that later in life could lead to hyperglycemia and diabetes in MODY3 and discovered that *HNF1A*+/R272C β cells hypersecrete INS. We provide evidence in support of hyperinsulinemia being caused by deregulation of K_{ATP} channels in the β cells and that this is partly mediated by HNF4A. Finally, we show that INS hypersecretion can be rescued by pharmacologically targeting K_{ATP} and low-voltage-gated calcium channels.

RESULTS

Generation of a human disease model for MODY3

To establish a human disease model of MODY3, we derived patient-specific hiPSC lines by reprogramming dermal fibroblasts from a MODY3 patient carrying a heterozygous R272C mutation in the DNA-binding domain of *HNF1A*. The R272C mutation is a dominant-negative mutation that abrogates both the DNA-binding and transactivation activities of HNF1A.[21] Several *HNF1A*+/R272C hiPSC clones retained a pluripotent morphology for more than 10 passages, and we used two clones for this study (1-mut and 2-mut). Two isogenic control lines were established from each of these clones (1-corA, 1-corB and 2-corA, 2-corB) (Figures 1A, 1B, and S1A–S1D) by CRISPR-Cas9 genome editing.[22] All hiPSC lines expressed hallmark pluripotency factors and spontaneously differentiated into the three germ layers in embryoid bodies (Figures S1E and S1F; data not shown). We further confirmed a normal karyotype, silencing of the lentiviral-expressed reprogramming factors and single integration of the targeting vectors (Figures S1G–S1I).

MODY3 patient-specific hiPSCs differentiate normally to glucose-responsive β cells

Although HNF1A plays an essential role in GSIS in mature β cells,[23] its expression is initiated already in pancreatic progenitors.[24] To explore potential developmental deficits of *HNF1A*+/R272C cells, we used a 7-stage directed β cell differentiation protocol with minor adjustments (Figure S2A).[25] The second isogenic hiPSC set required optimization of the protocol (1-day extensions of S2 and S4) to enable NKX6-1 induction (data not shown). Analyses of the expression of crucial pancreatic transcription factors and the main pancreatic hormones at the pancreatic progenitor stage (S4) and at the β cell stage (S7) revealed that *HNF1A*+/R272C cells are fully capable of differentiating into β cells (Figures 1C–1E, S2B–S2E, S3A, and S3B). As expected, based on the nature of the mutation, *HNF1A* was expressed at comparable levels in the *HNF1A*+/R272C cells compared with corrected controls throughout the differentiation protocol (Figures S2E and S3A).

Importantly, all cell lines robustly differentiated to C-peptide+ (CPEP+)/NKX6-1+ β cells (on average 34%–39% and 27%–29% of the total cell population for the cell lines of the first and second isogenic sets, respectively) (Figures 1D, 1E, and S3B). The α-to-β cell ratio was unaltered, while the δ-to-β cell ratio was increased in the corrected control cells compared with the mutant cells in one of the two isogenic hiPSC sets (Figures 1F and S3C–S3E). Accordingly, the INS and glucagon

---

Figure 1. Specification of β cells from MODY3 hiPSCs is unperturbed

(A) Schematic of the MODY3 disease model generation, where two patient-specific *HNF1A*+/R272C hiPSC clones (1-mut and 2-mut) were corrected to the wild-type genotype *HNF1A*+/corrected (1-corA, 1-corB, 2-corA, and 2-corB). Additionally, 2-mut was mock transfected in parallel with 2-corA and 2-corB to derive a second *HNF1A*+/R272C hiPSC clone (2-mut-subcl).

(B) Sanger sequencing reads of *HNF1A* show a heterozygous C-to-T point mutation causing the R272C (arginine-to-cysteine) mutation in the MODY3 patient-derived hiPSC line 1-mut and the correction of the mutation in the 1-corA and 1-corB isogenic control hiPSC lines.

(C) Representative immunofluorescence confocal images of S7 cells stained for NKX6-1 (yellow), GCG (cyan), CPEP (magenta), and DNA (blue) or CPEP (yellow), NKX-1 (cyan), PDX1 (magenta) and DNA (blue). Scale bars represent 250 μm (overview) or 25 μm (close ups).

(D) Representative flow cytometry density plots of the total (top) or CPEP+ (bottom) S7 population.

(E) Flow cytometry-based quantification of CPEP+/NKX6-1+ S7 cells. n = 7 independent experiments. Data are represented as mean +SD.

(F) Flow-cytometry-based quantification of the ratio of α cells (single GCG+ and double GCG+/CPEP+) to β cells (single CPEP+). n = 6 (1-corA and 1-corB) or 7 (1-mut) independent experiments. Data are represented as mean + SD.

(G) ELISA measurements of total INS content normalized to DNA content at S7. n = 9 (1-corB) or 10 (1-corA and 1-mut) independent experiments. Data are represented as mean + SD.

(H) ELISA measurements of total GCG content normalized to DNA content at S7. n = 6 (1-corB) or 7 (1-corA and 1-mut) independent experiments. Data are represented as mean + SD.
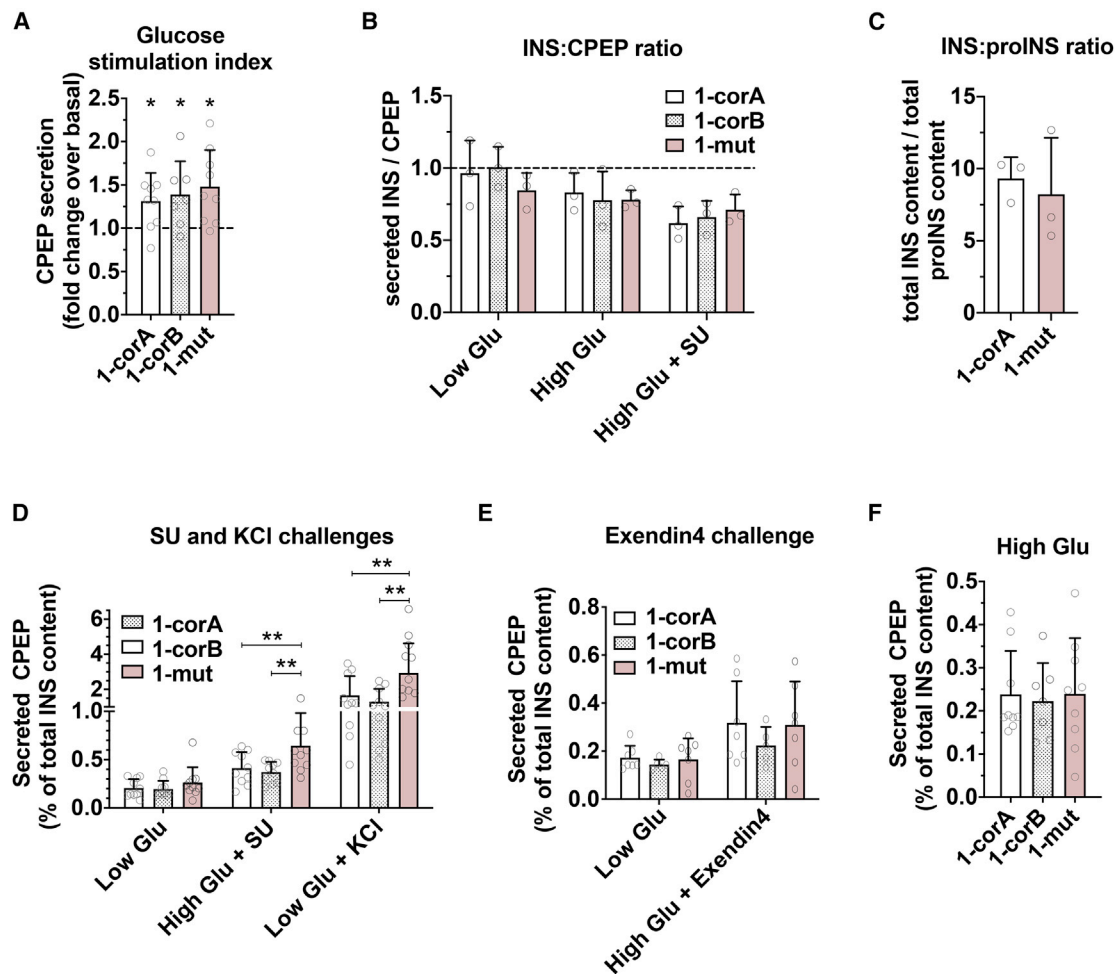
See also Figures S1–S3.

Figure 2. MODY3 hiPSC-derived β cells hypersecrete insulin *in vitro*

(A) The fold change of CPEP secretion in 30 min 16.67 mM glucose relative to 1.67 mM glucose of S7 cells. Asterisks indicate significance between low and high glucose. n = 7 (1-corB) or 9 (1-corA and 1-mut) independent experiments. Data are represented as mean + SD. Wilcoxon matched-pairs signed-rank test analysis.

(B) The ratio between secreted CPEP and INS (both in the same units) after 30 min in 1.67-mM glucose (low Glu), 16.67-mM glucose (high Glu), or 16.67-mM glucose with 100-μM tolbutamide (high Glu + SU) in S7 cells. n = 3 independent experiments.

(C) The ratio between total INS content to total proinsulin (proINS) content (both in the same units) in S7 cells. n = 3 independent experiments. Data are represented as mean + SD.

(D) ELISA measurements of secreted CPEP after 30 min in 1.67-mM glucose (low Glu), 16.67-mM glucose with 100-μM tolbutamide (high Glu + SU) or 1.67-mM glucose with 30-mM KCl (low Glu + KCl) normalized to total INS content in S7. n = 10 independent experiments. Data are represented as mean + SD. Wilcoxon matched-pairs signed-rank test analysis.

(E) ELISA measurements of secreted CPEP after 30 min in 1.67 or 16.67 mM glucose with exendin4 normalized to total INS content in S7 cells. n = 5 (1-corB) or 7 (1-corA and 1-mut) independent experiments. Data are represented as mean + SD.

(F) ELISA measurements of secreted CPEP after 30 min in 16.67-mM glucose normalized to total INS content in S7 cells. n = 7 (1-corB) or 9 (1-corA and 1-mut) independent experiments. Data are represented as mean + SD.

*, and ** represent statistical significance at p % 0.05, p % 0.01, respectively. See also Figure S3.

(GCG) contents were similar in mutant and corrected control cell lines (Figures 1G, 1H, S3F, and S3G). The difference in δ cell differentiation between mutant and corrected control lines was not consistent in the two hiPSC sets, suggesting that clonal variations rather than the *HNF1A-R272C* mutation explain this difference (Figure S3D).

Typically, MODY3 patients do not develop hyperglycemia and diabetes until adolescence.[7] The fact that GSIS was not compromised in *HNF1A*[+/R272C] β cells (Figures 2A and S3H) and that *in vitro*-generated β cells from hPSCs resemble

fetal β cells[26] suggest that our model captures a pre-diabetic stage.

Consistent with the previous data on MODY3 patient-specific hiPSC-derived β cells,[17] the ratios of secreted INS to CPEP and of the total INS to proinsulin content were unaltered in *HNF1A*[+/R272C] S7 cells *in vitro* (Figures 2B and 2C).

HNF1A[+/R272C] β cells hypersecrete insulin

Since MODY3 patients are hyperresponsive to SUs compared with other diabetic patients,[6,20] we tested whether our *in vitro*
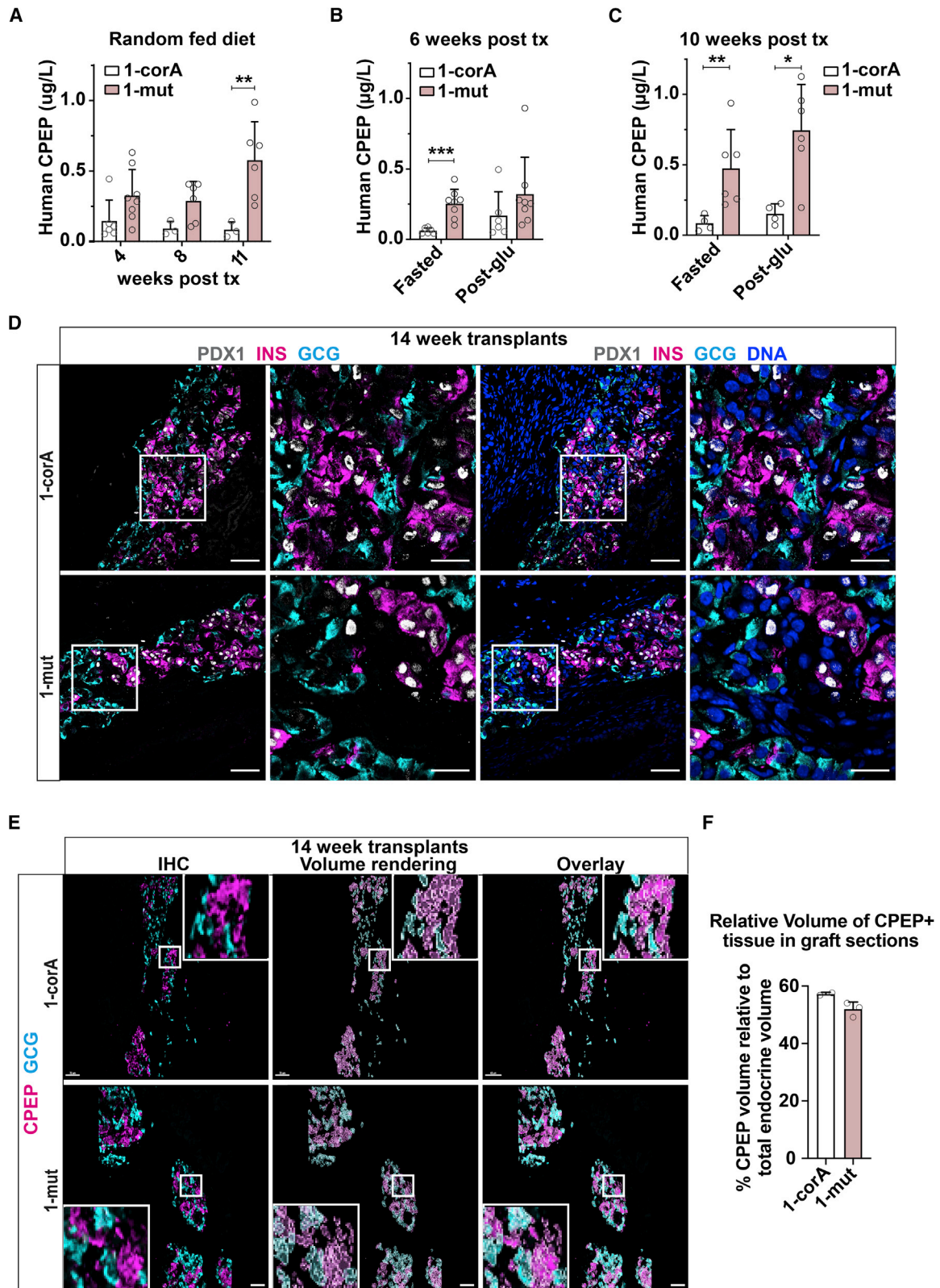
(legend on next page)

model would recapitulate the sensitivity of patients to SUs. Surprisingly, $HNF1A^{+/R272C}$ β cells from both hiPSC isogenic sets displayed increased INS secretion in response to the SU compound tolbutamide in the presence of high glucose compared with the corrected controls (Figures 2D and S3I). Consistently, $HNF1A^{+/R272C}$ β cells also hypersecreted INS in response to challenges with the depolarizing agent potassium chloride (KCl) compared with the corrected controls, but not in response to the GLP1 analog Exendin4 (Figures 2D, 2E, and S3I). In low-glucose conditions, there was an overall trend for $HNF1A^{+/R272C}$ β cells to hypersecrete INS in vitro, whereas for high glucose there was no difference (Figures 2D, 2F, and S3I). While SUs mainly act via the closure of K_{ATP} channels and consequential membrane depolarization,[5] GLP1 analogs amplify INS granule exocytosis via cAMP production.[27] Hence, our findings suggest that the cell membrane of $HNF1A^{+/R272C}$ is more sensitive to depolarizing stimuli compared to control β cells.

We further aimed to validate the hypersecretion phenotype of $HNF1A^{+/R272C}$ β cells in a more physiological relevant in vivo niche. We therefore transplanted corrected control and mutant S7 cells under the kidney capsule of immunocompromised mice. The function of the engrafted S7 cells were tested 4 to 11 weeks post-transplantation by measuring circulating human CPEP in serum samples taken from mice carrying grafts of either corrected control or mutant S7 cells. Importantly, the $HNF1A^{+/R272C}$ grafts displayed significantly increased INS secretion both in fasted conditions from 6 weeks post-transplantation, and in glucose-challenged and random fed conditions from 10 weeks post-transplantation (Figures 3A–3C). At 14 weeks post-transplantation INS$^+$/GCG$^-$ and GCG$^+$/INS$^-$ cells were observed in clusters in both $HNF1A^{R272C/+}$ and corrected control grafts (Figure 3D). Quantification of the number of β cells showed no significant difference between $HNF1A^{R272C/+}$ and corrected control grafts, indicating that the hyperinsulinemia could not be explained by a survival advantage conveyed by the $HNF1A^{+/R272C}$ mutation (Figures 3E and 3F; Table S1). Taken together, these findings indicate that INS hypersecretion precedes $HNF1A^{+/R272C}$ β cell failure.

$HNF1A^{+/R272C}$ β cells display dysregulated expression of membrane potential regulators

To elucidate the underlying mechanism for INS hypersecretion in $HNF1A^{+/R272C}$ β cells, we analyzed the transcriptomes of sorted CPEP$^+$/NKX6-1$^+$ β cells by RNA sequencing (Figures 4A and S4A). Principal-component analysis (PCA) separated the transcriptomes of $HNF1A^{+/R272C}$ and corrected control β cells in PC1 (explaining 69% of the variance), which indicates that the genotype is the primary source of variance (Figure S4B). We identified 410 downregulated and 281 upregulated genes in the $HNF1A^{+/R272C}$ β cells (Figure S4C). In line with recent transcriptomic data on MODY3 patient islets and in vitro-generated β cells with HNF1A null mutations,[16,17,28] we found and validated the downregulation of MODY transcription factors (NEUROD1, HNF4A, and PAX4) and the δ cell hormone (SST). Furthermore, regulators of INS secretion (DPEP1, DPP4, IAPP, and IGF2), glucose transport (SLC2A2) and glycolysis (PKLR and G6PC2) were downregulated (Figures 4B, S4D, and S4E). Dysregulation of these genes may contribute to the ultimate development of an INS secretion defect in MODY3 patients, but it cannot directly explain the observed INS hypersecretion phenotype.

On the contrary, gene set enrichment analysis identified an overrepresentation of ion transport and membrane potential regulators (Figures 4C, 4D, and S4F). These gene expression changes could result in increased INS secretion via perturbed membrane potential. We validated the altered expression of a subset of potassium channels (KCNA3, KCNK9, and HCN1), calcium channels (CACNA1B), and K_{ATP} channel regulators (SRC and ANK2) in $HNF1A^{+/R272C}$ β cells by RT-qPCR (Figure 4B). Although the RNA sequencing showed no change in the expression of the SU target, the main K_{ATP} channel in β cells (Figure S4G), reexamination by RT-qPCR analysis revealed reduced expression of both subunits, ABCC8 (SUR1) and KCNJ11 (Kir6.2), in $HNF1A^{+/R272C}$ β cells (Figure 4B). RT-qPCR analysis also showed downregulation of a potassium channel (KCNH6) and an intracellular calcium channel (ATP2A3) in $HNF1A^{+/R272C}$ β cells, confirming previous studies based on hESC-derived β cells carrying HNF1A null mutations (Figure 4B).[16,17]

In silico analysis predicted NEUROD1- and HNF4A-binding motifs within 2 kb of the transcriptional start site of all validated ion channels, membrane potential regulators and MODY transcription factors, while HNF1A binding motifs were present only on NEUROD1 and HNF4A (Figure S5A). Also, it is a well-known fact that HNF4A mutations lead to INS hypersecretion in MODY1 prior to diabetes onset.[9,30] We therefore hypothesized that NEUROD1 and HNF4A could work as potential downstream effectors of HNF1A. To test this hypothesis, we first confirmed reduced expression of NEUROD1 and HNF4A proteins in HNF1A$^{+/R272C}$ CPEP$^+$/NKX6-1$^+$ β cells (Figures S5B–S5F). Next, we knocked down NEUROD1 or HNF4A expression in S7 corrected control cells using shRNA and siRNA, respectively.

Figure 3. MODY3 hiPSC-derived β cells hypersecrete insulin in vivo

(A–E) Severe combined immunodeficiency-beige (SCID-BEIGE) mice transplanted with 1-mut or 1-corA S7 cells under the kidney capsule.

(A–C) Secreted human CPEP measurements from blood samples of random fed mice (A) at 4, 8, and 11 weeks post-transplantation (post tx) and of fasted and glucose-challenged mice at 6 weeks (B) and 10 weeks (C) post-transplantation. n = 3 (1-corA, week 8 and 11), 4 (1-corA, week 10), 6 (1-corA, week 4 and 6; 1-mut, week 4, 10, and 11), or 8 (1-mut, week 4 and 6) mice. Data are represented as mean + SD. A Mann-Whitney test was used to assess significance. *, **, and *** represent statistical significance at p ⩽ 0.05, p ⩽ 0.01, and p ⩽ 0.001, respectively.

(D) Representative immunofluorescence confocal images of 14-week transplants stained for PDX1 (gray), CPEP (magenta), and GCG (cyan). Scale bars represent 50 and 20 μm (insets).

(E) Representative immunofluorescence confocal images of 14-week transplants stained for CPEP (magenta) and GCG (cyan); left panels show immunofluorescence stainings, middle panels show volume renderings (segmented with Imaris image analysis software), right panels show an overlay of immunofluorescence staining and volume renderings. Scale bars represent 70 μm.

(F) Image-based quantification of the volume of CPEP$^+$ tissue relative to total endocrine tissue (GCG$^+$ and INS$^+$) on each imaged section. Data points represent the average of two confocal z stacks of 10-μm sections for each graft. Data are represented as mean + SEM. n = 2 (1-corA) or 3 (1-mut) mice.
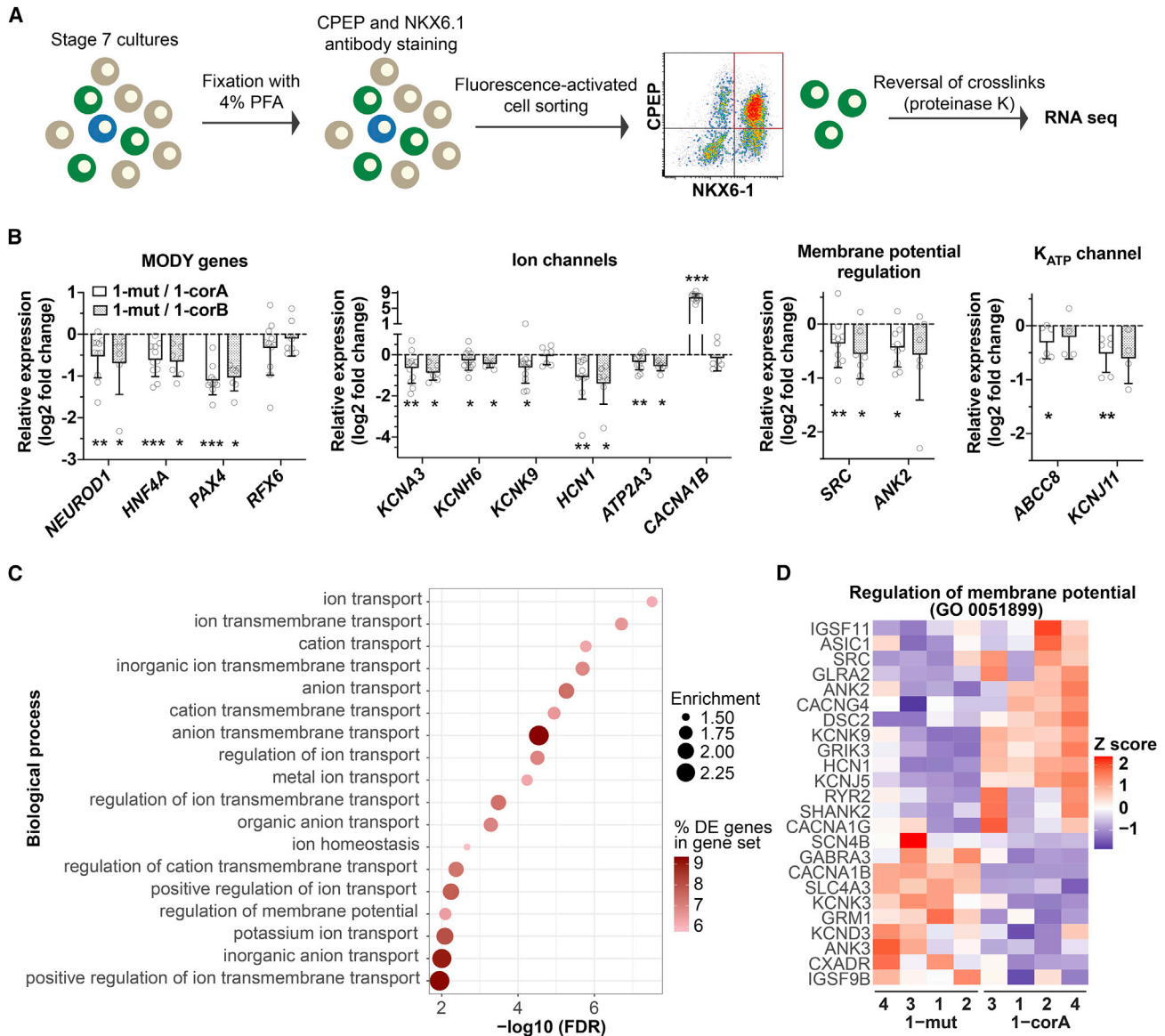
See also Table S1.

Figure 4. Membrane potential-related genes are deregulated in MODY3 β cells

(A) Schematic of the purification of CPEP+/NKX6-1+ S7 β cells (green) from 1-corA and 1-mut lines by MARIS (method for analyzing RNA following intracellular sorting)[29] prior to bulk RNA sequencing. n = 4 independent experiments.

(B) RT-qPCR of CPEP+/NKX6-1+ S7 cells assessing MODY genes (*NEUROD1*, *HNF4A*, *PAX4*, and *RFX6*), ion channels (*KCNA3*, *KCNH6*, *KCNK9*, *HCN1*, *ATP2A3*, and *CACNA1B*), membrane potential regulators (*SRC* and *ANK2*), and the K$_{ATP}$ subunits (*ABCC8* and *KCNJ11*). n = 7 (1-corB) or 12 (1-corA and 1-mut) independent experiments. Data are represented as mean + SD. Wilcoxon matched-pairs signed-rank test analysis. *, **, and *** represent statistical significance at p % 0.05, p % 0.01, and p % 0.001, respectively.

(C) Overrepresented GO terms related to ion transport and membrane potential regulation within the RNA sequencing dataset.

(D) Heatmap of differentially expressed genes from the GO term "regulation of membrane potential." The S7 cells were generated in four independent experiments (1–4).

See also Figures S4 and S5.

Based on the RT-qPCR results (Figure S5G), we conclude that NEUROD1 may mediate the reduced expression of *SST*, *PAX4*, and a subset of ion channels (e.g., *KCNA3*, *KCNA6*, and *ATP2A3*) downstream of HNF1A in MODY3, but not the subunits of the main K$_{ATP}$ channel in β cells: *ABCC8* and *KCNJ11*. Thus, NEUROD1's role as an effector of HNF1A in MODY3 is not central to early INS hypersecretion but rather could contribute to INS

insufficiency and diabetes later in life. Interestingly, knocking down *HNF4A* resulted in reduced expression of the SU target, *ABCC8*, suggesting that HNF4A may act as a downstream mediator of hyperinsulinemia in HNF1A+/R272C β cells (Figure S5H).

Taken together, the observed gene expression changes of membrane potential regulators and ion channels, including the K$_{ATP}$ channel, could lead to decreased membrane conductance
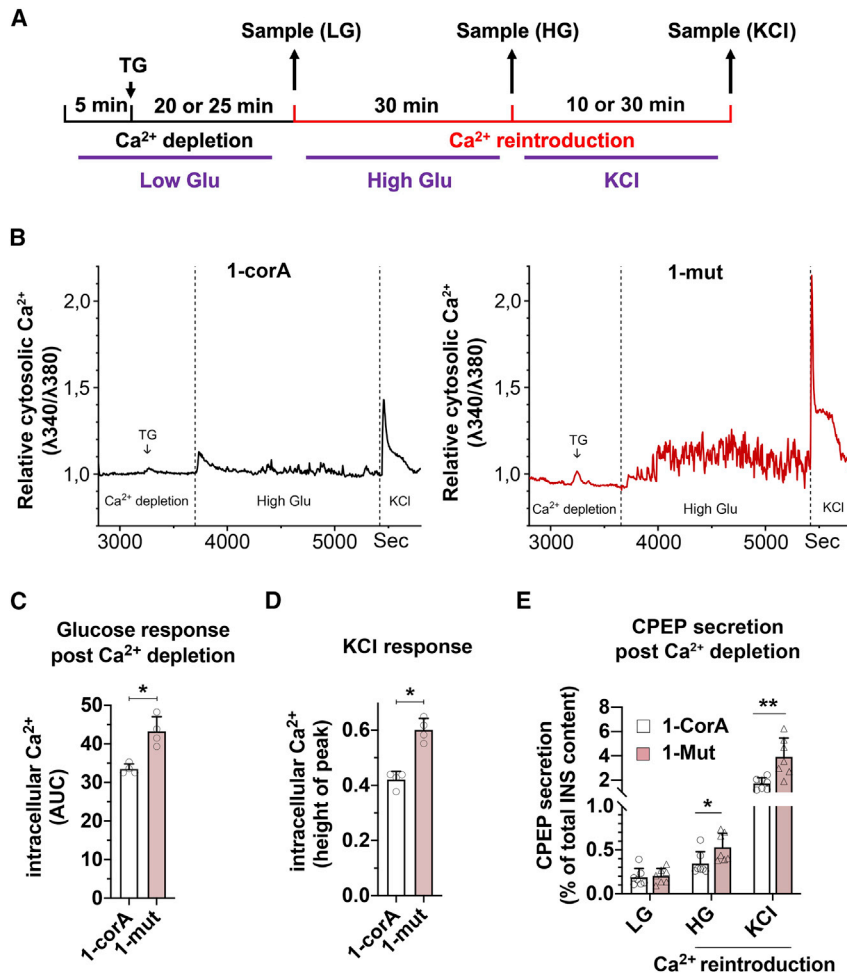
A

B

C

D

E

Figure 5. Increased calcium signaling in MODY3 β cells

(A) Schematic of experimental setup for Ca^{2+} depletion in low glucose (0 mM Ca^{2+}; 1.67 mM glucose; 5 μM thapsigargin to empty intracellular Ca^{2+} stores) and Ca^{2+} reintroduction with high glucose (2.2 mM Ca^{2+}; 16.7 mM glucose) and KCl (2.2 mM Ca^{2+}; 16.7 mM glucose; 30 mM KCl) challenges. The setup was used for Ca^{2+} imaging (B–D; 25 min low Glu and 10 min KCl) or ELISA measurements of CPEP secretion (E; 30 min low Glu and 30 min KCl), and the schematic includes the ELISA sampling scheme. TG, thapsigargin.

(B) Representative tracks of single, live-imaged S7 cells (1-mut and 1-corA) loaded with an intracellular calcium dye (Fura2-AM) showing relative cytosolic intracellular Ca^{2+} levels.

(C and D) Bar graphs showing the area under the curve (AUC) during the high glucose challenge (C) and the height of the peak in response to KCl (D). A Mann-Whitney test was used to assess significance. n = 4 independent experiments (each data point is the mean of 38–73 cells). Data are represented as mean + SD.

(E) ELISA measurements of secreted CPEP after 30 min with Ca^{2+} depletion (no Ca^{2+}) in 1.67-mM glucose (LG), Ca^{2+} reintroduction (2.2 mM Ca^{2+}) with 16.67-mM glucose (HG), and 1.67-mM glucose with 30-mM KCl (KCl) in S7 cells normalized to total INS content. n = 7 independent experiments. Data are represented as mean + SD. Wilcoxon matched pairs signed-rank test analysis.

*, **, and *** represent statistical significance at p % 0.05, p % 0.01, and p % 0.001, respectively. See also Figure S6.

for K^+ ions and increased cytosolic concentrations of Ca^{2+} ions. Consequently, this could lead to increased membrane excitability, since the required depolarization stimulus for reaching the action potential threshold would be reduced. Hence, our gene expression analysis uncovers membrane potential regulation as a likely pathway underlying INS hypersecretion in $HNF1A^{+/R272C}$ β cells.

$HNF1A^{+/R272C}$ endocrine cells show increased calcium signaling

In β cells, INS secretion is induced by Ca^{2+} influx that is facilitated by voltage-activated calcium channels whose activity depends on the membrane potential. We assessed the intracellular Ca^{2+} dynamics on a single-cell level as a proxy for membrane potential changes. Intracellular Ca^{2+} dynamics of S7 cultures were determined during glucose and KCl challenges after initially depleting the cells of Ca^{2+} (Figure 5A). We focused on the endocrine cells by using a clear response to the depolarization agent KCl as inclusion criteria. Upon reintroducing Ca^{2+} and elevating the glucose concentration, there was an immediate surge in cytosolic Ca^{2+} in mutant and isogenic control cells due to the strong electrochemical gradient for Ca^{2+} entry. Thereafter, approximately 25% of both mutant and control cells continued oscillating, which suggested that similar subsets of glucose-responsive β cells

were present among the endocrine cells in these cell lines (Figures 5B and S6A). However, the $HNF1A^{+/R272C}$ cells displayed increased calcium signaling during the glucose challenge (measured by the area under the curve; Figure 5C). In addition, the amplitude in response to depolarization by KCl was increased in the $HNF1A^{+/R272C}$ cells (Figure 5D). We also analyzed the effect of shifting from low to high glucose prior to calcium depletion and reintroduction under high glucose conditions. Consistent with the GSIS data (Figure 2D), calcium signaling was unaffected under these basal conditions (Figure S6B; data not shown). Altogether, the increased calcium signals in $HNF1A^{+/R272C}$ single endocrine cells indicate more efficient membrane depolarization, which could be the upstream mechanism of INS hypersecretion.

To strengthen our conclusion that increased calcium signaling leads to INS hypersecretion in $HNF1A^{+/R272C}$ cells, CPEP secretion measurements revealed a significant INS hypersecretion phenotype upon Ca^{2+} reintroduction in $HNF1A^{+/R272C}$ cells compared with corrected control cells (Figures 5A and 5E).

Increased birth weight in $HNF1A^{+/G292FS}$ mutation carriers and pharmacological rescue of insulin hypersecretion in $HNF1A^{+/R272C}$ β cells

The observed INS hypersecretion phenotype in $HNF1A^{+/R272C}$ β cells is reminiscent of congenital hyperinsulinemia (CHI),
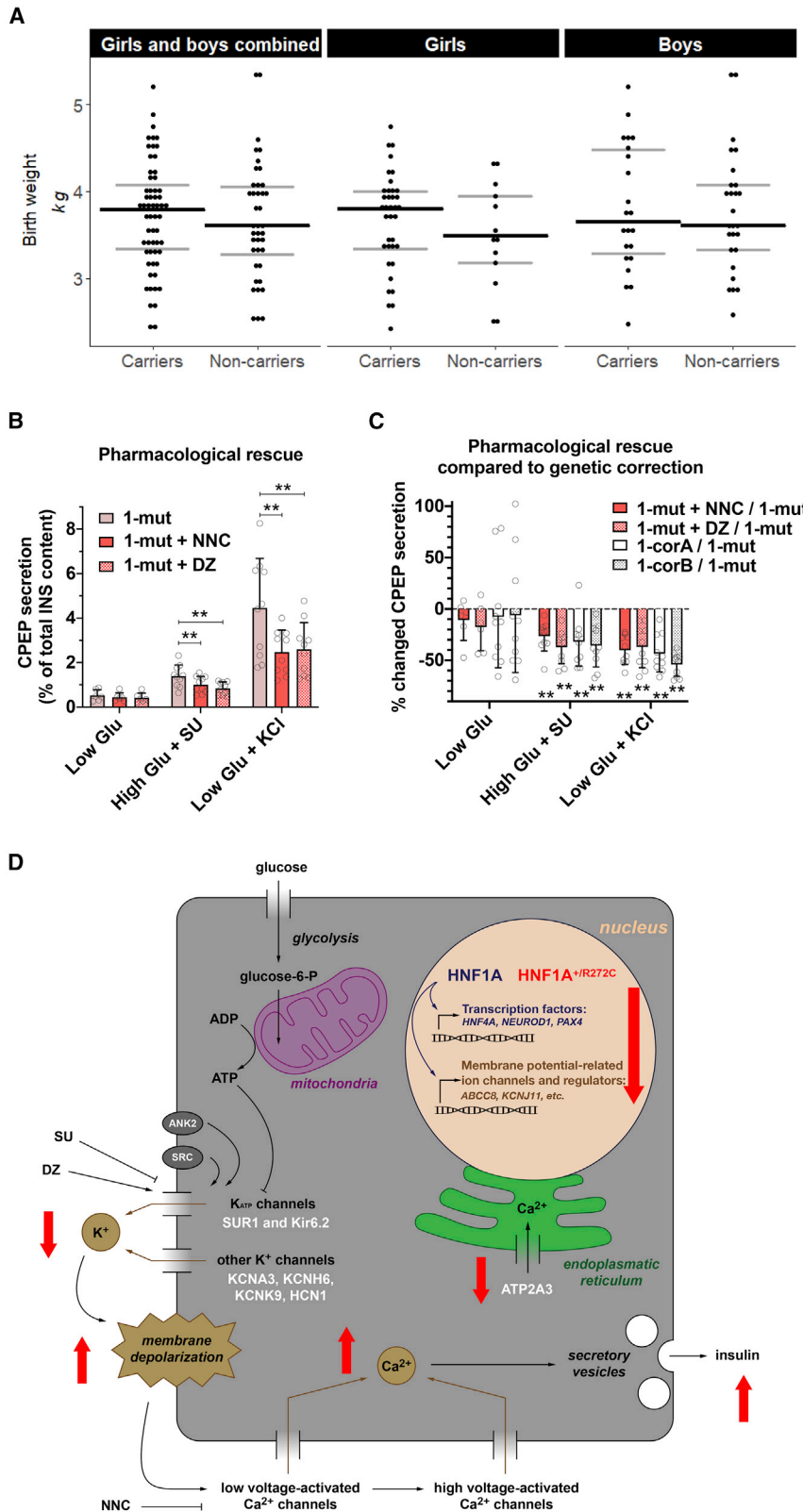
Figure 6. *HNF1A* mutation carriers show increased birth weight and rescue of insulin hypersecretion by pharmacological targeting of calcium and potassium channels

(A) Median birth weight of heterozygous G292fs (glycine-to-frameshift) *HNF1A* mutation carriers and sibling non-carriers. Interquartile ranges are indicated. n = 41 (non-carriers, 13 girls and 28 boys) or 58 (carriers, 35 girls and 23 boys) individuals.

(B) ELISA measurements of CPEP secretion after 30 min in 1.67-mM glucose (low Glu), 16.7-mM glucose with 100-μM tolbutamide (high Glu + SU) and 1.67-mM glucose with 30-mM KCl (low Glu + KCl), without (1-mut) or with the addition of 100-μM potassium channel activator diazoxide (1-mut + DZ) and 1-μM low-voltage-gated calcium channel blocker NNC55-0396 (1-mut + NNC), normalized to total INS content in S7. n = 6 (low Glu) or 10 (high Glu +SU and low Glu +KCl) independent experiments. Data are represented as mean + SD. Wilcoxon matched pairs signed-rank test analysis.

(C) The CPEP secretion changes by treating 1-mut with NNC and DZ (related to Figure 5B) or correcting the R272C mutation (related to Figure 2D). Asterisks indicate a significant difference to 1-mut. n = 6 (1-mut + NNC/1-mut, low Glu; 1-mut + DZ/1-mut, low Glu) or 10 (rest of data) independent experiments. Data are represented as mean + SD. Wilcoxon matched pairs signed-rank test analysis.

(D) Model illustrating the proposed mechanism underlying insulin hypersecretion in $HNF1A^{+/R272C}$ β cells (red arrows indicate direction of dysregulations). We propose that insulin hypersecretion in $HNF1A^{+/R272C}$ β cells is mediated via altered expression of potassium and calcium channels, in particular via reduced expression of the K_{ATP} subunits Kir6.2 (*KCNJ11*) and SUR1 (*ABCC8*), where *HNF4A* may mediate the effect on SUR1. In cooperation with downregulation of the K_{ATP} regulators *ANK2* and *SRC*, reduced expression of Kir6.2 and SUR1 is likely to lead to an overall decreased conductance of K^+ ions, which will depolarize the membrane potential and thereby reduce the stimulus required to reach the voltage threshold for low voltage-activated calcium channel activation. As a result, the influx of Ca^{2+} ions is increased, and this altered calcium homeostasis in turn leads to increased insulin secretion. Another downstream target of HNF1A in MODY3, NEUROD1, mediates the reduced expression of *SST*, *PAX4*, and a subset of ion channels, which may contribute to insulin insufficiency and diabetes later in life of MODY3 patients.

*, **, and *** represent statistical significance at p % 0.05, p % 0.01, and p % 0.001, respectively.

which has been reported for *HNF4A* mutation carriers.[9] For *HNF4A* mutation carriers, it is well established that CHI is accompanied by an increased birth weight, likely due to the anabolic effects of INS.[9,31] This led us to retrospectively analyze the birth weight data from a Finish MODY3 cohort carrying a heterozygous G292fs mutation in *HNF1A*.[8] There was a trend of an increased median birth weight in *HNF1A*[+/G292FS] newborns (3.78 kg, 35 girls and 23 boys) compared with non-carrier family members (3.58 kg, 13 girls and 28 boys) (Figure 6A), consistent with a conceivable mild neonatal hyperinsulinemia phenotype in *HNF1A*[+/G292FS] newborns.

The K_{ATP} channel activator diazoxide is used as treatment of severe CHI.[31,32] The T-type calcium channel blocker NNC55-0396 (NNC) blocks the low-voltage-activated calcium channels, which amplify small depolarization stimuli.[33] We therefore assessed whether these pharmacological agents attenuated INS secretion in *HNF1A*[+/R272C] β cells. Indeed, both NNC and diazoxide rescued the INS hypersecretion that we observed during SU and KCl challenges in *HNF1A*[+/R272C] β cells (Figure 6B). The decrease in INS secretion in treated *HNF1A*[+/R272C] β cells was very similar to what was obtained in the untreated genetically corrected isogenic control lines (Figure 6C). In addition to providing targeted treatment candidates, these data support a model of MODY3, in which increased membrane excitability underlies INS hypersecretion (Figure 6D).

DISCUSSION

We used MODY3 patient-specific hiPSCs (*HNF1A*[+/R272C]) and isogenic corrected controls in conjunction with directed β cell differentiation as a model to study the early pathogenesis of MODY3. As a proof of principle for our disease model, we recapitulated the specific responsiveness of β cells in MODY3 patients to K_{ATP} channel blockers (SUs). Importantly, our MODY3 cellular model indicates that INS hypersecretion—the hallmark of CHI—precedes β cell failure in MODY3.

The known CHI-causing genes, with few exceptions, encode components of the membrane potential triggering pathway, with mutations in the main β cell K_{ATP} channel being the most common cause.[34–36] Indeed, we observed reduced expression of the two K_{ATP} subunits *ABCC8* and *KCNJ11* encoding the SU receptor 1 (SUR1) and the inward rectifying potassium channel (Kir6.2), respectively, in HNF1A[+/R272C] β cells. In addition, the expression of K_{ATP} regulators (*ANK2* and *SRC*) and other membrane potential-related ion channels (*KCNA3*, *KCNA6*, *KCNK9*, *HCN1*, and *ATP2A3*) were reduced in *HNF1A*[+/R272C] β cells. Initially, *in silico* analysis and a previous enhancer binding study[37] suggested NEUROD1 as a potential downstream mediator of HNF1A. However, while knockdown of *NEUROD1* in corrected control β cells reduced the expression of a subset of the ion channels (*KCNA3*, *KCNA6*, and *ATP2A3*) and *PAX4*, it failed to mimic the INS hypersecretion phenotype of *HNF1A*[+/R272C] β cells. Consistently, neither the K_{ATP} subunits *ABCC8* and *KCNJ11* nor their regulators *SRC* and *ANK2* were affected upon the *NEUROD1* knockdown.

Mutations in *HNF4A* (MODY1) are associated with INS hypersecretion in neonates through an unknown mechanism.[9] Since the expression of *HNF4A* is reduced in *HNF1A*[+/R272C] β cells,

we knocked down the expression of *HNF4A* in corrected control β cells to test whether it mediates reduced expression of the K_{ATP} channel downstream of *HNF1A*. Indeed, *ABCC8* expression was reduced in *HNF4A* knockdown β cells. Based on our data, we propose a model where *HNF1A* mutations, partially via HNF4A, result in INS hypersecretion via reduced K_{ATP} channel activity, which leads to decreased membrane conductance of K$^+$ ions causing increased membrane excitability, Ca^{2+} ion influx and eventually increased INS secretion (Figure 6D). Notably, the proposed disease mechanism is supported by both the sensitivity to SU and the rescue of the INS hypersecretion with diazoxide in HNF1A[+/R272C] β cells, since SU and diazoxide bind directly to SUR1 to close and open the K_{ATP} channel, respectively.

We substantiate our INS hypersecretion model with clinical data by showing a trend of increased birth weight in a Finnish MODY3 family cohort, which is indicative of CHI. Our findings are corroborated by case reports of *HNF1A* mutation carriers suffering from CHI in the neonatal period of life.[13,31,38] To our knowledge, this link between a perturbed membrane potential and CHI in *HNF1A* mutation carriers has so far not been described.

HNF1A typically acts as a homodimer, and the protein contains an N-terminal dimerization domain, a DNA-binding domain (where the R272C mutation is located), and a C-terminal transactivation domain. Mutations in the dimerization and DNA-binding domains have been associated with an earlier diagnosis of diabetes, likely due to the dominant-negative nature of a subset of these mutations, conferring a severe reduction in functional HNF1A dimers.[7,21] In contrast, the Finnish cohort harbored the G293fs mutation leading to a truncated protein, lacking the transactivation domain. Thus, the tendency of increased birth weight (indicative of CHI) in the Finnish cohort was perhaps less severe than in carriers with dominant-negative mutations. Interestingly, the majority of CHI-causing *HNF1A* mutations have been located to the dimerization or the DNA-binding domain.[31,32,38] Among the reported CHI subjects, one patient carried a R272H mutation,[31] indicating that the arginine in position 272 plays a crucial role for proper function of HNF1A and that its loss gives rise to a phenotype in the severe end of the spectrum.

The identification of mechanisms that can mediate glucose sensing and INS release in β cells downstream of *HNF1A* highlights the benefits of hiPSC disease models. However, a fundamental question remains—how does CHI relate to the development of diabetes in *HNF1A* mutation carriers? Hyperinsulinemia and hyperglycemia could be two independent phenotypes due to pleiotropic roles of HNF1A, or hyperinsulinemia could be the primary cause of the development of hyperglycemia. Although MODY3 β cells show gene expression changes consistent with hyperglycemia and hypersecretion of INS, the only phenotype detectable in hiPSC-derived MODY3 β cells is hypersecretion of INS, suggesting that deficient INS secretion is secondary to hyperinsulinemia. This model is also supported by the disease progression observed for case reports of MODY patients carrying inactivating mutations in *ABCC8*, which is among the most common causes of CHI.[36] For *ABCC8* patients, it was proposed that hyperinsulinemia transitions into hyperglycaemia through increased intracellular Ca^{2+} levels and

increased INS secretion.[39] We not only observed elevated intracellular Ca^{2+} levels, but also deregulation of the sarcoplasmic/endoplasmic reticulum calcium ATPase 1 (SERCA) pump *ATP2A3*, which have previously been linked to apoptosis and desensitization of the INS secretion machinery, contributing to the development of diabetes.[30,40,41] Hence, our data suggest that hyperinsulinemia likely precipitates progressive hyperglycaemia.

However, our MODY3 hiPSC model also identified factors whose perturbed expression could predispose *HNF1A* mutation carriers to hyperglycaemia, such as transcription factors fundamental to β cell identity and function (NEUROD1, HNF4A, and PAX4).[42–44] Similarly, perturbed expression of glycolysis-related enzymes (PKLR and G6PC2)—that couple glucose sensing to INS secretion—could also predispose for *HNF1A*-mediated hyperglycaemia. It is therefore conceivable that these gene expression changes also contribute to disease onset.

Interestingly, González et al.[17] recently used patient-derived haploinsufficient *HNF1A* mutant hiPSC lines with a different mutation (R200Q) to reveal progressive loss of β cell function. Although $HNF1A^{+/R200Q}$ β cells secreted INS normally *in vitro*, they were unable to compensate for higher metabolic INS demands *in vivo* due to the gradual development of INS secretory defects.[17]

The most common treatment of mild neonatal hyperinsulinemia is extra feeding. However, feeding does not target the primary cause of hyperinsulinemia but simply alleviates the symptoms of hyperinsulinemia, namely hypoglycemia.[31,32] Thus, it is conceivable that a therapeutic treatment of even mild hyperinsulinemia to prevent increased intracellular Ca^{2+} levels may be advantageous for delaying or even preventing diabetes onset. Importantly, we find that the potassium channel activator diazoxide and the low-voltage-activated calcium channel inhibitor NNC rescue the INS hypersecretion phenotype. Thereby, we identify these pharmacological agents as potential targeted treatments of hyperinsulinemia in *HNF1A* mutation carriers.

In conclusion, our study highlights the importance of patient-specific hiPSCs as a platform for studying early disease mechanisms that pave the way for personalized medicine. Our results emphasize the importance of early identification of the type of *HNF1A* mutation and a need for further investigation into the relationship between treatment of hyperinsulinemia in neonates and a potential delay of diabetes onset.

Limitations of the study
In this study, two sets of patient-specific $HNF1A^{+/R272C}$ and isogenic corrected control hiPSC-derived β cells were studied *in vitro* and *in vivo*. As MODY3 can be caused by many mutations and is known as a disease with heterogeneous phenotypes, the discovered INS hypersecretion phenotype cannot, at this point, be claimed to be the unifying primary defect in MODY3. Additionally, future studies have to address how INS hypersecretion transitions to an INS secretion defect. Finally, the sample size of the birth weight data of $HNF1A^{+/G292FS}$ mutation carriers was too low for statistical analysis.

STAR★METHODS

Detailed methods are provided in the online version of this paper and include the following:

- KEY RESOURCES TABLE
- RESOURCE AVAILABILITY
  - Lead contact
  - Materials availability
  - Data and code availability
- EXPERIMENTAL MODEL AND SUBJECT DETAILS
  - Patient samples, patient birth weight data, and ethics statement
  - hiPSC derivation, maintenance
  - Genetic correction of mutant iPS cell lines
  - The use of animals
- METHOD DETAILS
  - Spontaneous embryoid body differentiation
  - Differentiation of hiPSCs towards β cells
  - Immunofluorescence imaging *in vitro*
  - Flow cytometry
  - RT-qPCR
  - Stimulated insulin secretion assays and pharmacological rescue
  - RNA extraction of fixed and sorted cells
  - RNA sequencing and bioinformatics analysis
  - Transplantation of S7 β cells
  - Intraperitoneally glucose challenge
  - Histology and immunofluorescence staining of grafts
  - Analysis of the graft by immunofluorescence staining
  - Calcium imaging
  - Stimulated insulin secretion assays during Calcium depletion and reintroduction
  - *In Silico* transcription factor binding analysis
  - siRNA knockdown of HNF4A
  - shRNA knockdown of NEUROD1
- QUANTIFICATION AND STATISTICAL ANALYSIS

REFERENCES

1. Kim, S.H. (2015). Maturity-onset diabetes of the young: what do clinicians need to know? Diabetes Metab. J. *39*, 468–477. https://doi.org/10.4093/dmj.2015.39.6.468.

2. Lehto, M., Tuomi, T., Mahtani, M.M., Widén, E., Forsblom, C., Sarelin, L., Gullström, M., Isomaa, B., Lehtovirta, M., Hyrkkö, A., et al. (1997). Characterization of the MODY3 phenotype. Early-onset diabetes caused by an insulin secretion defect. J. Clin. Invest. *99*, 582–591. https://doi.org/10.1172/JCI119199.

3. Pontoglio, M., Prié, D., Cheret, C., Doyen, A., Leroy, C., Froguel, P., Velho, G., Yaniv, M., and Friedlander, G. (2000). HNF1alpha controls renal glucose reabsorption in mouse and man. EMBO Rep. *1*, 359–365. https://doi.org/10.1093/embo-reports/kvd071.

4. Shepherd, M., Shields, B., Ellard, S., Rubio-Cabezas, O., and Hattersley, A.T. (2009). A genetic diagnosis of HNF1A diabetes alters treatment and improves glycaemic control in the majority of insulin-treated patients. Diabet. Med. *26*, 437–441. https://doi.org/10.1111/j.1464-5491.2009.02690.x.

5. Lv, W., Wang, X., Xu, Q., and Lu, W. (2020). Mechanisms and characteristics of sulfonylureas and glinides. Curr. Top. Med. Chem. *20*, 37–56. https://doi.org/10.2174/1568026620666191224141617.

6. Pearson, E.R., Starkey, B.J., Powell, R.J., Gribble, F.M., Clark, P.M., and Hattersley, A.T. (2003). Genetic cause of hyperglycaemia and response to treatment in diabetes. Lancet *362*, 1275–1281. https://doi.org/10.1016/S0140-6736(03)14571-0.

7. Bellanné-Chantelot, C., Carette, C., Riveline, J.P., Valéro, R., Gautier, J.F., Larger, E., Reznik, Y., Ducluzeau, P.H., Sola, A., Hartemann-Heurtier, A., et al. (2008). The type and the position of HNF1A mutation modulate age at diagnosis of diabetes in patients with maturity-onset diabetes of the young (MODY)-3. Diabetes *57*, 503–508. https://doi.org/10.2337/db07-0859.

8. Kettunen, J.L.T., Rantala, E., Dwivedi, O.P., Isomaa, B., Sarelin, L., Kokko, P., Hakaste, L., Miettinen, P.J., Groop, L.C., and Tuomi, T. (2022). A multi-generational study on phenotypic consequences of the most common causal variant of HNF1A-MODY. Diabetologia *65*, 632–643. https://doi.org/10.1007/s00125-021-05631-z.

9. Pearson, E.R., Boj, S.F., Steele, A.M., Barrett, T., Stals, K., Shield, J.P., Ellard, S., Ferrer, J., and Hattersley, A.T. (2007). Macrosomia and hyperinsulinaemic hypoglycaemia in patients with heterozygous mutations in the HNF4A gene. PLoS Med. *4*, e118. https://doi.org/10.1371/journal.pmed.0040118.

10. Kettunen, J.L.T., and Tuomi, T. (2020). Human physiology of genetic defects causing beta-cell dysfunction. J. Mol. Biol. *432*, 1579–1598. https://doi.org/10.1016/j.jmb.2019.12.038.

11. Dukes, I.D., Sreenan, S., Roe, M.W., Levisetti, M., Zhou, Y.P., Ostrega, D., Bell, G.I., Pontoglio, M., Yaniv, M., Philipson, L., and Polonsky, K.S. (1998). Defective pancreatic beta-cell glycolytic signaling in hepatocyte nuclear factor-1alpha-deficient mice. J. Biol. Chem. *273*, 24457–24464. https://doi.org/10.1074/jbc.273.38.24457.

12. Párrizas, M., Maestro, M.A., Boj, S.F., Paniagua, A., Casamitjana, R., Gomis, R., Rivera, F., and Ferrer, J. (2001). Hepatic nuclear factor 1-alpha directs nucleosomal hyperacetylation to its tissue-specific transcriptional targets. Mol. Cell. Biol. *21*, 3234–3243. https://doi.org/10.1128/MCB.21.9.3234-3243.2001.

13. Shih, D.Q., Screenan, S., Munoz, K.N., Philipson, L., Pontoglio, M., Yaniv, M., Polonsky, K.S., and Stoffel, M. (2001). Loss of HNF-1alpha function in mice leads to abnormal expression of genes involved in pancreatic islet development and metabolism. Diabetes *50*, 2472–2480. https://doi.org/10.2337/diabetes.50.11.2472.

14. McCulloch, L.J., van de Bunt, M., Braun, M., Frayn, K.N., Clark, A., and Gloyn, A.L. (2011). GLUT2 (SLC2A2) is not the principal glucose transporter in human pancreatic beta cells: implications for understanding genetic association signals at this locus. Mol. Genet. Metab. *104*, 648–653. https://doi.org/10.1016/j.ymgme.2011.08.026.

15. Servitja, J.M., Pignatelli, M., Maestro, M.A., Cardalda, C., Boj, S.F., Lozano, J., Blanco, E., Lafuente, A., McCarthy, M.I., Sumoy, L., et al. (2009). Hnf1alpha (MODY3) controls tissue-specific transcriptional programs and exerts opposed effects on cell growth in pancreatic islets and liver. Mol. Cell. Biol. *29*, 2945–2959. https://doi.org/10.1128/MCB.01389-08.

16. Cardenas-Diaz, F.L., Osorio-Quintero, C., Diaz-Miranda, M.A., Kishore, S., Leavens, K., Jobaliya, C., Stanescu, D., Ortiz-Gonzalez, X., Yoon, C., Chen, C.S., et al. (2019). Modeling monogenic diabetes using human ESCs reveals developmental and metabolic deficiencies caused by mutations in HNF1A. Cell Stem Cell *25*. 273–289.e5. https://doi.org/10.1016/j.stem.2019.07.007.

17. González, B.J., Zhao, H., Niu, J., Williams, D.J., Lee, J., Goulbourne, C.N., Xing, Y., Wang, Y., Oberholzer, J., Blumenkrantz, M.H., et al. (2022). Reduced calcium levels and accumulation of abnormal insulin granules in stem cell models of HNF1A deficiency. Commun. Biol. *5*, 779. https://doi.org/10.1038/s42003-022-03696-z.

18. Low, B.S.J., Lim, C.S., Ding, S.S.L., Tan, Y.S., Ng, N.H.J., Krishnan, V.G., Ang, S.F., Neo, C.W.Y., Verma, C.S., Hoon, S., et al. (2021). Decreased GLUT2 and glucose uptake contribute to insulin secretion defects in MODY3/HNF1A hiPSC-derived mutant beta cells. Nat. Commun. *12*, 3133. https://doi.org/10.1038/s41467-021-22843-4.

19. Cujba, A.M., Alvarez-Fallas, M.E., Pedraza-Arevalo, S., Laddach, A., Shepherd, M.H., Hattersley, A.T., Watt, F.M., and Sancho, R. (2022). An HNF1alpha truncation associated with maturity-onset diabetes of the young impairs pancreatic progenitor differentiation by antagonizing HNF1beta function. Cell Rep. *38*, 110425. https://doi.org/10.1016/j.celrep.2022.110425.

20. Østoft, S.H., Bagger, J.I., Hansen, T., Pedersen, O., Faber, J., Holst, J.J., Knop, F.K., and Vilsbøll, T. (2014). Glucose-lowering effects and low risk of hypoglycemia in patients with maturity-onset diabetes of the young when treated with a GLP-1 receptor agonist: a double-blind, randomized, crossover trial. Diabetes Care *37*, 1797–1805. https://doi.org/10.2337/dc13-3007.

21. Yoshiuchi, I., Yamagata, K., Yang, Q., Iwahashi, H., Okita, K., Yamamoto, K., Oue, T., Imagawa, A., Hamaguchi, T., Yamasaki, T., et al. (1999). Three new mutations in the hepatocyte nuclear factor-1alpha gene in Japanese subjects with diabetes mellitus: clinical features and functional characterization. Diabetologia *42*, 621–626. https://doi.org/10.1007/s001250051204.

22. Cong, L., Ran, F.A., Cox, D., Lin, S., Barretto, R., Habib, N., Hsu, P.D., Wu, X., Jiang, W., Marraffini, L.A., and Zhang, F. (2013). Multiplex genome engineering using CRISPR/Cas systems. Science *339*, 819–823. https://doi.org/10.1126/science.1231143.

23. Pontoglio, M., Sreenan, S., Roe, M., Pugh, W., Ostrega, D., Doyen, A., Pick, A.J., Baldwin, A., Velho, G., Froguel, P., et al. (1998). Defective insulin secretion in hepatocyte nuclear factor 1alpha-deficient mice. J. Clin. Invest. 101, 2215–2222. https://doi.org/10.1172/JCI2548.

24. Nammo, T., Yamagata, K., Tanaka, T., Kodama, T., Sladek, F.M., Fukui, K., Katsube, F., Sato, Y., Miyagawa, J., and Shimomura, I. (2008). Expression of HNF-4alpha (MODY1), HNF-1beta (MODY5), and HNF-1alpha (MODY3) proteins in the developing mouse pancreas. Gene Expr. Patterns 8, 96–106. https://doi.org/10.1016/j.modgep.2007.09.006.

25. Rezania, A., Bruin, J.E., Arora, P., Rubin, A., Batushansky, I., Asadi, A., O'Dwyer, S., Quiskamp, N., Mojibian, M., Albrecht, T., et al. (2014). Reversal of diabetes with insulin-producing cells derived in vitro from human pluripotent stem cells. Nat. Biotechnol. 32, 1121–1133. https://doi.org/10.1038/nbt.3033.

26. Nair, G.G., Liu, J.S., Russ, H.A., Tran, S., Saxton, M.S., Chen, R., Juang, C., Li, M.L., Nguyen, V.Q., Giacometti, S., et al. (2019). Recapitulating endocrine cell clustering in culture promotes maturation of human stem-cell-derived beta cells. Nat. Cell Biol. 21, 263–274. https://doi.org/10.1038/s41556-018-0271-4.

27. Leech, C.A., Dzhura, I., Chepurny, O.G., Kang, G., Schwede, F., Genieser, H.G., and Holz, G.G. (2011). Molecular physiology of glucagon-like peptide-1 insulin secretagogue action in pancreatic beta cells. Prog. Biophys. Mol. Biol. 107, 236–247. https://doi.org/10.1016/j.pbiomolbio.2011.07.005.

28. Haliyur, R., Tong, X., Sanyoura, M., Shrestha, S., Lindner, J., Saunders, D.C., Aramandla, R., Poffenberger, G., Redick, S.D., Bottino, R., et al. (2019). Human islets expressing HNF1A variant have defective beta cell transcriptional regulatory networks. J. Clin. Invest. 129, 246–251. https://doi.org/10.1172/JCI121994.

29. Hrvatin, S., Deng, F., O'Donnell, C.W., Gifford, D.K., and Melton, D.A. (2014). MARIS: method for analyzing RNA following intracellular sorting. PLoS One 9, e89459. https://doi.org/10.1371/journal.pone.0089459.

30. Arya, V.B., Rahman, S., Senniappan, S., Flanagan, S.E., Ellard, S., and Hussain, K. (2014). HNF4A mutation: switch from hyperinsulinaemic hypoglycaemia to maturity-onset diabetes of the young, and incretin response. Diabet. Med. 31. e11–e15. https://doi.org/10.1111/dme.12369.

31. Rozenkova, K., Malikova, J., Nessa, A., Dusatkova, L., Bjørkhaug, L., Obermannova, B., Dusatkova, P., Kytnarova, J., Aukrust, I., Najmi, L.A., et al. (2015). High incidence of heterozygous ABCC8 and HNF1A mutations in Czech patients with congenital hyperinsulinism. J. Clin. Endocrinol. Metab. 100, E1540–E1549. https://doi.org/10.1210/jc.2015-2763.

32. Snider, K.E., Becker, S., Boyajian, L., Shyng, S.L., MacMullen, C., Hughes, N., Ganapathy, K., Bhatti, T., Stanley, C.A., and Ganguly, A. (2013). Genotype and phenotype correlations in 417 children with congenital hyperinsulinism. J. Clin. Endocrinol. Metab. 98, E355–E363. https://doi.org/10.1210/jc.2012-2169.

33. Braun, M., Ramracheya, R., Bengtsson, M., Zhang, Q., Karanauskaite, J., Partridge, C., Johnson, P.R., and Rorsman, P. (2008). Voltage-gated ion channels in human pancreatic beta-cells: electrophysiological characterization and role in insulin secretion. Diabetes 57, 1618–1628. https://doi.org/10.2337/db07-0991.

34. Güemes, M., Rahman, S.A., Kapoor, R.R., Flanagan, S., Houghton, J.A.L., Misra, S., Oliver, N., Dattani, M.T., and Shah, P. (2020). Hyperinsulinemic hypoglycemia in children and adolescents: recent advances in understanding of pathophysiology and management. Rev. Endocr. Metab. Disord. 21, 577–597. https://doi.org/10.1007/s11154-020-09548-7.

35. Kapoor, R.R., Flanagan, S.E., Arya, V.B., Shield, J.P., Ellard, S., and Hussain, K. (2013). Clinical and molecular characterisation of 300 patients with congenital hyperinsulinism. Eur. J. Endocrinol. 168, 557–564. https://doi.org/10.1530/EJE-12-0673.

36. Stanley, C.A. (2016). Perspective on the genetics and diagnosis of congenital hyperinsulinism disorders. J. Clin. Endocrinol. Metab. 101, 815–826. https://doi.org/10.1210/jc.2015-3651.

37. Tennant, B.R., Robertson, A.G., Kramer, M., Li, L., Zhang, X., Beach, M., Thiessen, N., Chiu, R., Mungall, K., Whiting, C.J., et al. (2013). Identification and analysis of murine pancreatic islet enhancers. Diabetologia 56, 542–552. https://doi.org/10.1007/s00125-012-2797-5.

38. Stanescu, D.E., Hughes, N., Kaplan, B., Stanley, C.A., and De León, D.D. (2012). Novel presentations of congenital hyperinsulinism due to mutations in the MODY genes: HNF1A and HNF4A. J. Clin. Endocrinol. Metab. 97, E2026–E2030. https://doi.org/10.1210/jc.2012-1356.

39. Huopio, H., Otonkoski, T., Vauhkonen, I., Reimann, F., Ashcroft, F.M., and Laakso, M. (2003). A new subtype of autosomal dominant diabetes attributable to a mutation in the gene for sulfonylurea receptor 1. Lancet 361, 301–307. https://doi.org/10.1016/S0140-6736(03)12325-2.

40. Efanova, I.B., Zaitsev, S.V., Zhivotovsky, B., Köhler, M., Efendić, S., Orrenius, S., and Berggren, P.O. (1998). Glucose and tolbutamide induce apoptosis in pancreatic beta-cells. A process dependent on intracellular Ca2+ concentration. J. Biol. Chem. 273, 33501–33507. https://doi.org/10.1074/jbc.273.50.33501.

41. Zarain-Herzberg, A., García-Rivas, G., and Estrada-Avilés, R. (2014). Regulation of SERCA pumps expression in diabetes. Cell Calcium 56, 302–310. https://doi.org/10.1016/j.ceca.2014.09.005.

42. Gu, C., Stein, G.H., Pan, N., Goebbels, S., Hörnberg, H., Nave, K.A., Herrera, P., White, P., Kaestner, K.H., Sussel, L., and Lee, J.E. (2010). Pancreatic beta cells require NeuroD to achieve and maintain functional maturity. Cell Metab. 11, 298–310. https://doi.org/10.1016/j.cmet.2010.03.006.

43. Hansen, S.K., Párrizas, M., Jensen, M.L., Pruhova, S., Ek, J., Boj, S.F., Johansen, A., Maestro, M.A., Rivera, F., Eiberg, H., et al. (2002). Genetic evidence that HNF-1alpha-dependent transcriptional control of HNF-4alpha is essential for human pancreatic beta cell function. J. Clin. Invest. 110, 827–833. https://doi.org/10.1172/JCI15085.

44. Sosa-Pineda, B., Chowdhury, K., Torres, M., Oliver, G., and Gruss, P. (1997). The Pax4 gene is essential for differentiation of insulin-producing beta cells in the mammalian pancreas. Nature 386, 399–402. https://doi.org/10.1038/386399a0.

45. Ran, et al. (2013). "Genome engineering using the CRISPR-Cas9 system". Nat. Protoc. 8, 2281–2308. https://doi.org/10.1038/nprot.2013.143.

46. Schindelin, J., Arganda-Carreras, I., Frise, E., Kaynig, V., Longair, M., Pietzsch, T., Preibisch, S., Rueden, C., Saalfeld, S., Schmid, B., et al. (2012). Fiji: an open-source platform for biological-image analysis. Nat. Methods 9, 676–682. https://doi.org/10.1038/nmeth.2019.

47. Rérat, M., and Pouchan, C. (1994). Dynamic scalar and tensor polarizabilities of the 2 (1)P and 2 (3)P states of He. Phys. Rev. A 49, 829–832. https://doi.org/10.1103/physreva.49.829.

48. Korotkevich, G., Sukhov, V., Budin, N., Shpak, B., Artyomov, M.N., and Sergushichev, A. (2021). Fast gene set enrichment analysis. Preprint at bioRxiv. https://doi.org/10.1101/060012.

49. Wickham, H. (2009). ggplot2 : Elegant Graphics for Data Analysis (Springer).

50. Daily, K., Patel, V.R., Rigor, P., Xie, X., and Baldi, P. (2011). MotifMap: integrative genome-wide maps of regulatory motif sites for model species. BMC Bioinformatics 12, 495. https://doi.org/10.1186/1471-2105-12-495.

51. Xie, X., Rigor, P., and Baldi, P. (2009). MotifMap: a human genome-wide map of candidate regulatory motif sites. Bioinformatics 25, 167–174. https://doi.org/10.1093/bioinformatics/btn605.

52. Maherali, N., Ahfeldt, T., Rigamonti, A., Utikal, J., Cowan, C., and Hochedlinger, K. (2008). A high-efficiency system for the generation and study of human induced pluripotent stem cells. Cell Stem Cell 3, 340–345. https://doi.org/10.1016/j.stem.2008.08.003.

53. Nostro, M.C., Sarangi, F., Yang, C., Holland, A., Elefanty, A.G., Stanley, E.G., Greiner, D.L., and Keller, G. (2015). Efficient generation of NKX6-1+ pancreatic progenitors from multiple human pluripotent stem cell lines. Stem Cell Rep. 4, 591–604. https://doi.org/10.1016/j.stemcr.2015.02.017.

54. Sui, L., Danzl, N., Campbell, S.R., Viola, R., Williams, D., Xing, Y., Wang, Y., Phillips, N., Poffenberger, G., Johannesson, B., et al.

(2018). β-cell replacement in mice using human type 1 diabetes nuclear transfer embryonic stem cells. Diabetes *67*, 26–35. https://doi.org/10.2337/db17-0120.

55. Ran, F.A., Hsu, P.D., Wright, J., Agarwala, V., Scott, D.A., and Zhang, F. (2013). Genome engineering using the CRISPR-Cas9 system. Nat. Protoc. *8*, 2281–2308. https://doi.org/10.1038/nprot.2013.143.

56. Olsen, L.R., Hansen, N.B., Bonde, M.T., Genee, H.J., Holm, D.K., Carlsen, S., Hansen, B.G., Patil, K.R., Mortensen, U.H., and Wernersson, R. (2011). PHUSER (Primer Help for USER): a novel tool for USER fusion primer design. Nucleic Acids Res. *39*, W61–W67. https://doi.org/10.1093/nar/gkr394.

57. D'Haene, B., Vandesompele, J., and Hellemans, J. (2010). Accurate and objective copy number profiling using real-time quantitative PCR. Methods *50*, 262–270. https://doi.org/10.1016/j.ymeth.2009.12.007.

58. Lithovius, V., Saarimäki-Vire, J., Balboa, D., Ibrahim, H., Montaser, H., Barsby, T., and Otonkoski, T. (2021). SUR1-mutant iPS cell-derived islets recapitulate the pathophysiology of congenital hyperinsulinism. Diabetologia *64*, 630–640. https://doi.org/10.1007/s00125-020-05346-7.

59. Millman, J.R., Xie, C., Van Dervort, A., Gürtler, M., Pagliuca, F.W., and Melton, D.A. (2016). Generation of stem cell-derived beta-cells from patients with type 1 diabetes. Nat. Commun. *7*, 11463. https://doi.org/10.1038/ncomms11463.

60. Bray, N.L., Pimentel, H., Melsted, P., and Pachter, L. (2016). Near-optimal probabilistic RNA-seq quantification. Nat. Biotechnol. *34*, 525–527. https://doi.org/10.1038/nbt.3519.

STAR★METHODS

KEY RESOURCES TABLE

REAGENT or RESOURCE	SOURCE	IDENTIFIER
Antibodies		
Anti-C-peptide (1:200)	DSHB	Cat#GN-ID4 (supernatant); RRID: AB_2255626
Anti-Proglucagon (1:250)	Cell signaling	Cat#8233s; RRID: AB_10859908
Anti-Somatostatin (1:1,000)	Santa Cruz	Cat#sc-7819; RRID: AB_2302603
Anti-PDX1 (1:500)	R&D systems	Cat#AF2419; RRID: AB_355257
Anti-NKX6-1 (1:500)	DSHB	Cat#F55A12 (concentrate); RRID: AB_532379
Anti-Oct3/4 (1:500)	Santa Cruz	Cat#sc-5279; RRID: AB_628051
Anti-Sox2 (1:200)	Abcam	Cat#ab59776; RRID: AB_945584
Anti-Nanog (1:400)	BD biosciences	Cat#N31-355; RRID: AB_1937305
Anti-Beta III tubulin (1:1,000)	Promega	Cat#G712A; RRID: AB_430874
Anti-AFP (1:500)	Dako	Cat#A0008; RRID: AB_2650473
Anti-SMA (1:100)	Dako	Cat#M0851; RRID: AB_2223500
Anti-NKX6-1 (1:200)	Novus Biologicals	Cat#NBP1-82553; RRID: AB_11023606
Anti-NEUROD1 (1:200)	Santa Cruz	Cat#sc-46684; RRID: AB_671759
Anti-HNF4A (1:200)	Santa Cruz	Cat#sc-8987; RRID: AB_2116913
Anti-MKi67 (1:200)	Abcam	Cat#ab15580; RRID: AB_443209
Anti-Rabbit-A647 (1:2,000 for FACS; 1:500 for immunofluorescence)	Thermo Fisher	Cat#A31573; RRID: AB_2536183
Anti- Rabbit-Cy3 (1:2,000 for FACS; 1:500 for immunofluorescence)	Jackson ImmunoReasearch	Cat#711-167-003; RRID: AB_2340606
Anti-Goat-Cy5 (1:2,000 for FACS; 1:500 for immunofluorescence)	Jackson ImmunoReasearch	Cat#705-175-147; RRID: AB_2340415
Anti-Rat-A488 (1:2,000 for FACS; 1:500 for immunofluorescence)	Thermo Fisher	Cat#A21208; RRID: AB_2535794
Anti-Mouse-A488 (1:2,000 for FACS; 1:500 for immunofluorescence)	Thermo Fisher	Cat#A21202; RRID: AB_141607
Anti-Mouse-Cy5 (1:2,000 for FACS; 1:500 for immunofluorescence)	Jackson ImmunoReasearch	Cat#715-175-151; RRID: AB_2340820
Bacterial strains		
MAX Efficiency DH5α T1 Phage Resistant Competent Cells	Thermo Fisher	Cat#12034013
Biological samples		
Human skin biopsies carrying a R272C mutation in *HNF1A*	Uppsala University	N/A

(Continued on next page)

Continued

REAGENT or RESOURCE	SOURCE	IDENTIFIER
Chemicals, peptides, and recombinant proteins		
CHIR99021	Axon Medchem	Cat#1386
Activin A	PeproTech	Cat#120-14
KGF	PeproTech	Cat#100-19
Vitamin C	Sigma Aldrich	Cat#A4403
LDN193189	Tebu Tech	Cat#04-0074-10
SANT1	Sigma Aldrich	Cat#S4572
Retinoic acid	Sigma Aldrich	Cat#R2625
TBP	Calbiochem	Cat#565740
ALK5iII	Santa Cruz	Cat#sc-221234A
γSECiI	VWR	Cat#565789
R428	Axon	Cat#1946
Trolox	Tocris Bioscience	Cat#6002
N-acetyl-cys	Sigma Aldrich	Cat#a9165
Heparin	Sigma Aldrich	Cat#H3149-100KU
Bovine serum albumin (BSA)	Proliant	Cat#7500804
Bovine serum albumin (BSA)	Sigma Aldrich	Cat#A7906
Y-27632	Merck Millipore	Cat#688000
45 % glucose solution in water	Sigma Aldrich	Cat#G8769
Tolbutamide	Sigma Aldrich	Cat#T0891
Exendin4	Sigma Aldrich	Cat#E7144
NNC55-0396	Sigma Aldrich	Cat#N0287
Diazoxide	Sigma Aldrich	Cat#D9035
Fura-2 AM	Thermo Fisher	Cat#F1221
Thapsigargin	Santa Cruz	Cat#sc-24017
Polybrene	Merck Millipore	Cat#TR-1003
Saponin	Sigma Aldrich	Cat#47036
Critical commercial assays		
RNeasy MiniKit	Qiagen	Cat#74106
Ultrasensitive C-peptide ELISA	Mercodia	Cat#10-1141-01
Ultrasensitive Insulin ELISA	Mercodia	Cat#10-1132-01
Glucagon ELISA	Mercodia	Cat#10-1271-01
LIVE/DEAD™ Fixable Violet Dead Cell Stain Kit	Thermo Fisher	Cat#L34955
RecoverAll Total Nucleic Acid Isolation Kit for FFPE	Thermo Fisher	Cat#AM1975
Qubit™ dsDNA HS assay kit	Thermo Fisher	Cat#Q32851
Lenti-X™ GoStix™ Plus kit	Takara	Cat#631280
Deposited data		
RNA-seq data	This paper	GEO: GSE193106
Experimental models: Cell lines		
HEK293T	This paper	N/A
HNF1A$^{+/R272C}$ hiPSC clones	This paper	N/A
HNF1A$^{+/R272C}$ corrected hiPSC clones	This paper	N/A
Experimental models: Organisms/strains		
Male CB17.Cg-Prkdc^{scid}Lyst^{bg-J}/Crl (SCID-BEIGE) mice	ScanburCharles River	Cat#250

(Continued on next page)

Continued

REAGENT or RESOURCE	SOURCE	IDENTIFIER
Oligonucleotides		
guideRNA: Target: HNF1A-exon4 (forward strand), GAC GTA CAG CGG GCC CCC CCC, PAM: AGG. G inserted upstream of the guideRNA sequence according to suggested design guidelines.[45] Off-set of 20 base pairs	This paper	N/A
GuideRNA: HNF1A-exon4 (reverse strand, specific for R272C mutation), GGA AGG CTT CTT CTT TGC AC, PAM: CGG.	This paper	N/A
negative control siRNA	Thermo Fisher	Cat#4392420
siRNA against *HNF4A*	Thermo Fisher	Cat#s6697, s6698
Recombinant DNA		
pX335-U6-Chimeric_BB-CBh-hSpCas9n	Cong et al.[22]	Addgene; Cat#42335;
NEUROD1 shRNA and shRNA Ctrl plasmids	OriGene	Cat#TL311201
Packaging plasmids	OriGene	Cat#TR30037
Software and algorithms		
FCS express 7	De Novo Software	https://denovosoftware.com
Fiji 2.0/ImageJ2	Schindelin et al.[46]	http://imagej.nih.gov/ij
Adobe Photoshop 2020	Adobe	https://www.adobe.com
Adobe Illustrator CC 2018	Adobe	https://www.adobe.com
R package "EgdeR"	Rerat and Pouchan[47]	https://bioconductor.org/packages/release/bioc/html/edgeR.html
R package "fgsea"	Korotkevich et al.[48]	https://bioconductor.org/packages/release/bioc/html/fgsea.html
R package "ggplot2"	Wickham et al.[49]	https://ggplot2.tidyverse.org
Imaris 8.4, 9.0	Bitplane	N/A
Origin (Student Version)	OriginLab	https://www.originlab.com
GraphPad (Version 7 and 8)	GraphPad by Dotmatics	https://www.graphpad.com
The Gene Search function of the online tool	Daily et al.[50] Xie et al.[51]	http://motifmap.ics.uci.edu

RESOURCE AVAILABILITY

Lead contact
Further information and requests for resources and reagents should be directed to and will be fulfilled by the lead contact, Henrik Semb (henrik.semb@helmholtz-muenchen.de).

Materials availability
All unique/stable reagents and the iPS cell lines generated in this study are available from the lead contact with a completed Materials Transfer Agreement.

Data and code availability
RNA-seq datasets (raw files and processed count matrices) collected in this study have been deposited at GEO under the accession number provided in the key resources table.

This paper does not report the original code. This study uses referenced sources of code that can be found in the vignettes of the cited packages. Details of the packages are provided in the key resources table, and the parameters are provided in the method details section. Any additional information required to reanalyze the data reported in this paper is available from the lead contact upon request.

EXPERIMENTAL MODEL AND SUBJECT DETAILS

Patient samples, patient birth weight data, and ethics statement
The protocol for skin biopsies was approved by the Regional Research Ethical Committee in Uppsala, Sweden, and written informed consent was obtained from the patient prior to the procedure. The Danish authorities approved reprogramming of human fibroblasts using lentiviruses ('Arbejdstilsynet') and animal experiments ('Miljø- og Fødevarestyrelsen – Dyreforsøgstilsynet').

The birth weight data of the Finnish family cohort was collected from the official growth charts, the birth certificates, or the national medical birth register as part of the PM9045858 and FINNMODY projects approved by the Ethics Committees of Medicine and Paediatrics of the Helsinki University Hospital.[8]

hiPSC derivation, maintenance

Skin punch biopsies (2 mm in diameter) were obtained in local anesthesia from a female donor, born in 1944, carrying an R272C mutation in *HNF1A*. The patient was diagnosed with MODY3 at the age of 38, but symptoms were already seen from the age of 12 years. Dermal fibroblast cells were maintained and reprogrammed according to a previously published protocol.[52] hiPSCs were cultured on human ESC-qualified Matrigel (Corning, cat# 734-0272) according to the manufacturer's protocol with daily changes of mTESR1™ medium (Stem Cell Technologies, cat# 85850) at 37° C and 5 % CO_2. Cells were passaged twice to three times weekly at subconfluency using TrypLE select (Thermo Fisher, cat# 12563011). The medium was supplemented with 10 μM ROCK inhibitor-Y-27632 (Merck Millipore, cat# 688000) on the first-day post passaging. HiPSCs were tested negative for mycoplasma in regular tests.

Genetic correction of mutant iPS cell lines

Wild-type hPSC control lines with dissimilar genetic backgrounds may mask a potential phenotype of a mutant line due to the variability in the efficiency of directed β cell differentiation protocols across hPSC lines.[53,54] Therefore, we corrected the mutation in two *HNF1A*[+/R272C] hiPSC clones (1-mut and 2-mut) by CRISPR-Cas9-facilitated genome editing[22] to obtain two isogenic control lines for each mutant clone (1-corA, 1-corB, 2-corA, 2-corB) (Figure 1A). Guide RNA sequences for double nicking were designed with a discontinued online tool from Feng Zhang's lab (see key resources table for guide RNA sequences). We chose a guide RNA specific for the mutation site, thus not targeting the WT allele. We assembled CRISPR-Cas9 nicking vectors using the px335 vector (Addgene, cat# 42335) following a published protocol.[22,55]

The targeting vector contained a 5' and a 3' homology arm of approximately 1.5 kb, wild-type DNA obtained from the wild-type allele of the 1-mut hiPSC line, and a neomycin selection cassette flanked by loxP sites. The fragments were assembled using the USER cloning approach.[56] The targeting vector was linearized before co-transfection with the CRISPR-Cas9 nicking vector using the P3 primary cell kit with the Nucleofector 4d X-unit (program CA137) with 6 μg targeting vector and 2.5 μg of each guide RNA. The 2-mut-subcl cell line was derived in parallel with the 2-corA and 2-corB corrected cell lines by using water instead of DNA in the transfection. The cells were initially cultured on irradiated mouse embryonic fibroblasts, and selection was initiated three to four days later using G418 at 40 ng/μl. The selection was maintained for 4 days after which fresh MEFs were added. 10-12 days after electroporation, single clonal colonies were picked and expanded. Correct targeting of clones was validated by PCR, restriction fragment length analysis using Hha1, and Sanger sequencing. The selection cassette was excised using CRE recombination from correctly targeted clones. The company Cell Guidance Systems performed karyotyping (20 G-banded metaphase spreads).

To exclude random integration of the targeting vector, the copy number of exon4 of HNF1A in the corrected control cells (1-corA and 1-corB) was determined by qRT-PCR as previously described.[57] In brief, a fragment of the targeting vector was amplified and quantified relative to the copy number of the single-copy reference genes *ZNF80* and *GPR15* using the amplification efficiency-adjusted DDCt method. The primer efficiencies were comparable (data not shown).

The use of animals

The use of mice for this research was approved by the University of Copenhagen Animal Care and Use Committee. All mice used in this study were taken care of and operated on according to the relevant regulations. Mice were healthy, housed, and cared for in individually ventilated cages (IVCs) on a standard 12 h light: 12 h dark cycle in the sterile Animal Facility at the Panum Campus, University of Copenhagen. Mice will be used after 7-10 days of acclimatization. Male SCID-BEIGE mice (Scanbur - Charles River) were aged 8 to 10 weeks at the time of transplantation.

METHOD DETAILS

Spontaneous embryoid body differentiation

Embryoid bodies were generated by mechanically dissecting hiPSC colonies into small chunks and transferring them to low-attachment plates. Embryoid bodies were kept in Knock-out DMEM media supplemented with 10 % FBS, 1x Non-Essential Amino Acids, and 1x GlutaMAX (all Thermo Fisher). After 7-10 days in suspension, embryoid bodies were plated onto 0.1 % gelatin-coated tissue culture plates and were allowed to attach and further spontaneously differentiate for another 7-10 days.

Differentiation of hiPSCs towards β cells

For pancreatic β cell differentiation, hiPSCs were dissociated as described above and seeded at a density of 120,000 (120 k) cells to 150 k cells per cm^2 on 12-well tissue culture plates coated with 1:30 diluted growth factor reduced matrigel (Corning, cat# BDAA356239) in mTESR1™ medium supplemented with 10 μM ROCK inhibitor-Y-27632 for the first day. Two days after seeding, differentiation was induced according to a published protocol,[25] with some modifications (Figure S2A): i) On the first day of stage 1 (S1), the media was devoid of BSA; ii) we used 100 ng/ml ActivinA instead of GDF8 throughout S1; iii) to reduce cell death, we shortened S6 to four days; iv) we kept the cells in 2D throughout the differentiation (no reseeding to liquid-air interphase); v) for the second isogenic hiPSC set (2-mut, 2-mut-subcl, 2-corA, 2-corB), we extended both S2 and S4 one day, since NKX6-1 expression in CPEP[+]

cells in this second set of isogenic cell lines was dependent on extending S2, and the CPEP⁺ / NKX6-1⁺ population further increased by additionally extending S4 with one day (data not shown).

Immunofluorescence imaging *in vitro*

Cells were fixed in 4 % PFA for 15-20 minutes (min) at room temperature, permeabilized in 0.5% Triton X-100 (v/v) in PBS for 15 min and blocked in 0.1% Triton X-100 in PBS supplemented with 5% normal donkey serum (Jackson ImmunoResearch, Cat# 017-000-121) (blocking buffer) for 1 hr at room temperature. The cells were incubated with primary antibodies in a blocking buffer overnight at 4°C. The next day, secondary antibodies diluted 1:500 in blocking buffer were applied for 1 hr at room temperature (see key resources table for antibody information). Cell nuclei were visualized by incubation with 5 μg/ml DAPI (Thermo Fisher Scientific, D1306) in PBS for 10 min. To enable confocal imaging of S7 cells, cells were dissociated for 5-7 min with TrypLE Select after one week in S7 and reseeded on 8-well μ-dishes (Ibidi, Cat# 80826) at a density of 300-500 k per cm² and cultured in S7 media for another week before fixation. Images used for quantifications were acquired on the same day of secondary antibody staining. ImageJ[46] was used to quantify NEUROD1 and HNF4A protein levels in CPEP⁺ / NKX6-1⁺ β cells. In brief, NKX6-1⁺ nuclei were segmented by smoothing the image, auto thresholding using the Huang algorithm, dilating, running a watershed, and analyzing particles between 40 and 300 μm². CPEP⁺ / NKX6-1⁺ cells were next determined by an average CPEP intensity above 1375 in the segmented nuclei (scattering of the cytoplasmic CPEP signal to the nucleus was achieved by opening the pinhole to 3.5 airy units). Cells were imaged on a wide-field Zeiss Axio Observer microscope or a confocal Zeiss LSM780 microscope.

Flow cytometry

The cells were dissociated to a single-cell suspension using TrypLE Select for 7-10 min and straining with 50 nm CellTrics filters (Sysmex, Cat# 04-004-2317). The cells were counted and fixed in 4 % formaldehyde (VWR, Cat# 9713.1000) for 15-20 min and stored in PBS with 1 % BSA (w/v) (Sigma, Cat# a7906) at 4° C until analysis. In a v-shaped 96-well format (Corning, Cat# 3894),250 k cells were permeabilized and blocked in PBS containing 0.2 % Triton X-100 (Sigma) and 5 % normal donkey serum for 30 min at 4° C. Subsequently, the cells were incubated with 100 μl blocking buffer with primary antibodies overnight at 4° C (see key resources table for antibody information). The next day, the cells were washed in PBS with 1 % BSA, incubated with 100 μl blocking buffer with secondary antibodies for 45 min at room temperature, and washed once more. The cells were analyzed on a BD LSRFortessa.

RT-qPCR

Total RNA was extracted using the RNeasy MiniKit (Qiagen, Cat# 74106). Reverse transcription was performed with SuperScript III (Thermo Fisher Scientific, cat# 18080085), according to the manufacturer's instructions, using 1.25 μM random hexamer and 1.25 μM oligo(dT) (Thermo Fisher Scientific). Real-time PCR measurements were performed in technical duplicates using the LightCycler 480II (Roche) with either POWERSYBR Green PCR Master Mix (Applied Biosystems) and 200 nM of each primer (validation of reprogramming and S1 to S5 time course analysis) or TaqMan™ FAM probes with TaqMan™ Master Mix (Thermo Fisher Scientific, Cat# 4364103) (all S7 samples). Relative gene expression was determined using the housekeeping genes ACTB or GAPDH for SYBR- or Taqman-based transcriptomic profiling, respectively (See Tables S2 and S3 for primer sequence and TaqMan™ probe information).

Stimulated insulin secretion assays and pharmacological rescue

After one week in S7, cells were dissociated for 5-7 min with TrypLE Select, reseeded on 24-well dishes at a density of 300-500 k per cm², and cultured in S7 media for another week. On the day of the stimulated insulin secretion assay, cells were washed twice with Krebs-Ringer bicarbonate buffer (KRB) containing 115 mM NaCl, 5 mM KCl, 1 mM MgCl₂, 2.2 mM CaCl₂, 20 mM HEPES, 24 mM NaHCO₃ and 0.2 % BSA (Sigma, Cat# a7906), and pH adjusted to 7.4. All subsequent incubation steps were carried out at 37°C and 5% CO2. For standard GSIS assays, the cells were pre-incubated for 1.5 hrs in KRB supplemented with 1.67 mM glucose, before consecutive 30 min incubations in the first KRB with low glucose (1.67 mM), then high glucose (16.67 mM), and finally low glucose with KCl (30 mM total). After each step, the medium was collected, and the cells were washed once with KRB. Variations of the protocol included the addition of 10 nM Exendin4 (Sigma, Cat# E7144) or 100 μM Tolbutamide (Sigma, Cat# T0891) in the high glucose step or the addition of either 1 μM NNC55-0396 (Sigma, Cat# N0287) or 100 μM Diazoxide (Sigma, D9035) throughout all steps. Appropriate concentrations of Exendin4, Tolbutamide, NNC55-0396, and Diazoxide have previously been published.[33,58,59] Finally, the cells were harvested, immediately transferred to ice, and sonicated in water for total DNA and hormone content quantifications. The samples for hormone content quantifications were diluted 2.5 times in 95% ethanol with 0.18 M HCl. All samples were stored at -80°C until analysis in technical duplicates with commercially available ELISA kits for secreted human CPEP, Insulin or Glucagon according to the manufacturer's recommendations (Mercodia, Cat# 10-1141-01, 10-1132-01 and 10-1271-01).

RNA extraction of fixed and sorted cells

The MARIS (method for analyzing RNA following intracellular sorting) protocol was adapted from a previously published protocol.[29] S7 cells were prepared for intracellular staining and flow cytometry as described above, with the following exceptions. The cells were kept in 15 ml Falcon tubes on ice during all steps after dissociation. Before fixation, the cells were stained for viability using LIVE/DEAD™ Fixable Violet Dead Cell Stain Kit according to the manufacturer's recommendation (Thermo Fisher Scientific, Cat# L34955). Cells were fixed and permeabilized with 4 % PFA containing 0.1 % saponin (Sigma, Cat# 47036) and 1 % RNasin Plus

RNase Inhibitor (Promega, Cat# N2615) for 30 min at 4° C. 0.1 % saponin and either 1 % or 0.5 % RNasin Plus RNase Inhibitor was maintained in all subsequent incubation or washing steps, respectively. The cells were incubated with primary antibodies in staining buffer supplemented with 1% BSA for 1 hour (hr). The sorting was carried out on a FACS Aria III (BD Biosciences) or a Sony SH800. Between 200 k and 1.2 million CPEP$^+$ / NKX6-1$^+$ cells were sorted per experiment, and RNA was isolated using the RecoverAll Total Nucleic Acid Isolation Kit for FFPE (Thermo Fisher Scientific, Cat# AM1975) according to the manufacturer's protocol. However, the initial protein digestion was prolonged from 15 min to 1 hr at 50°C.

RNA sequencing and bioinformatics analysis

The quality of RNA was checked using the Agilent Bioanalyzer 2100. The RIN values were between 4 and 5.4. 100 ng total RNA was subjected to cDNA synthesis and library construction using the Ovation® Human FFPE RNA seq library system (Nugen, cat. no. 0340 and 0341). Fragmentation was not carried out upon recommendation from the manufacturer. Otherwise, the standard protocol was followed. The library quality was assessed using Agilent Bioanalyzer dsDNA 1000 chip, and the library concentration was quantified using Qubit^{TM} dsDNA HS assay kit (Thermo Fisher Scientific). The library was loaded onto a high output flowcell FC-404-2005, and 75 base pairs single end sequencing was performed using Illumina NextSeq 500.

Between 41 and 48 million reads per sample were obtained. Reads from the Nextseq were converted to FASTQ-files using bcl2Fastq (Illumina) on a high-performance computing cluster. The quality of sequencing reads was assessed with FASTQC and deemed of suitable quality. Reads were mapped to the human genome Homo_sapiens.GRCh38.p13 built using Kallisto (v 0.42.5).[60] Differential expression was estimated using the R package EgdeR.[47] We corrected multiple comparisons, and genes with a false discovery rate (FDR) < 0.05 were extracted for further analysis. Significantly differentially expressed genes were tested for overrepresentation of assigned gene ontology terms (biological process and molecular function) versus all human genes as background using a hypergeometric test implemented in the R package fgsea.[48] Terms with an FDR < 0.05 were considered significantly regulated. Additional visualizations were generated using the R package ggplot2.[49]

Transplantation of S7 β cells

1.8 million S7 β cells per mouse were transplanted under the kidney capsule using a Transferpettor^{TM} (Brand®, 2.5–10 μl). Eight mice per experimental group were transplanted. Mice were anesthetized with Avertin (Sigma, Cat# T48402 and 240486, 500 mg/kg body weight, intraperitoneal). Carprofen was used as an analgesic during the operation until 24 hrs post-operation (5 mg/kg body weight subcutaneously).

The blood glucose and weight of the mice were monitored weekly. For blood glucose measurements, a handheld glucometer (Accu-Chek Aviva from Roche, Cat# 06988709170) was used, and blood was sampled from the tail by facial vein puncture using a 4 mm Goldenrod animal lancet. The blood was collected in non-heparinized Eppendorf tubes and allowed to clot at room temperature for 30 to 60 min. Subsequently, the blood was centrifuged for 10 min at 3000 g at 4° C, and the serum was collected and kept at minus 80° C until ELISA analysis.

Intraperitoneally glucose challenge

The IP glucose challenge was performed after a 5 hr morning fast. 2g glucose/kg of body weight was injected intraperitoneally (IP) in the form of a 45 % glucose solution in water (Sigma, Cat# G8769). Blood glucose levels were measured immediately before IP injection (time 0, post starvation), and 25 min after injection (time 25, post glucose). Blood samples for measuring human c-peptide levels were taken at time 0 and time 25.

Histology and immunofluorescence staining of grafts

At week 14 of the transplantation study, mice were sacrificed, and grafts were collected. During the experiment, five mice transplanted with control cells (1-corA) and two mice transplanted with mutant cells (1-mut) died. The death of the mice may have been connected to the brittle nature of the immunocompromised SCID-BEIGE mice. Both transplanted and non-transplanted kidneys were harvested, the latter to serve as a staining control. After fixation in 4 % PFA overnight at 4° C, kidney samples were processed for cryosectioning by incubating the samples sequentially in the following solutions for a minimum of 24 hrs at 4° C: PBS, 30 % Sucrose, 30 % sucrose and OCT (1:1 ratio), OCT. The samples were then put into fresh OCT and frozen in cryomoulds, ready for sectioning at a thickness of 10 μm onto superfrost plus slides. Prior to immunostainings, the slides were dried at room temperature for 30 min and washed in 1x PBS to remove OCT. Permeabilization was carried out in 0.1 % Tween20 in PBS for 5 min and blocked in 0.01 % Tween in PBS supplemented with 5 % normal donkey serum. The sections were incubated with primary antibodies diluted in 0.01 % Tween in PBS supplemented with 5 % normal donkey serum overnight at 4° C. On the following day, the sections were washed in 0.01 % Tween in PBS for 10 min followed by a wash in PBS. Hereafter, the sections were incubated with secondary antibodies diluted in PBS supplemented with 5 % normal donkey serum for 1 hr at room temperature. After a wash in PBS, the slides were mounted using fluorescence mounting medium with DAPI (Agilent). Immunofluorescence stainings were detected and analyzed on a Zeiss Axioplan 2 or with a Zeiss LSM780 confocal microscope. (See key resources table for antibody information.)

Analysis of the graft by immunofluorescence staining

To analyze β cell mass in kidney grafts post-transplant, 2 corrected control and 3 *HNF1A$^{+/R272C}$* grafts were analyzed. The volume of insulin- and glucagon-positive tissue was assessed. Two replicate IHC staining per graft was performed in the quantitative analysis.

All graft tissue was sectioned (10 μM sections) and stained by IHC for Insulin, Glucagon, and DAPI antigens as described above. Equal-sized tiles with a depth of 30 μM (1 μM per optical section) were acquired on the Zeiss 780 confocal microscope. For all acquired images, the surface function in Imaris was used to segment and quantify the volume of glucagon-positive or insulin-positive tissue. Cell debris and auto-fluorescent cells were removed manually to ensure the volume segmentation was faithful to true insulin/glucagon expression.

Calcium imaging
48 hrs prior to imaging, S7 cells were harvested as described above for flow cytometry. The cells were seeded in IBIDI μ-dishes, 35 mm, high (IBIDI, cat#81156) at a density between 200 k and 400 k cells/cm2. 16 hours prior to imaging, the glucose concentration in the S7 medium was reduced to 1.67 mM. Subsequently, the cells were incubated for 30 min with 5 μM Fura-2 AM (Thermo Fisher Scientific, Cat# F1221) in the presence of 0.1 % pluronic F127 and 1.67 mM glucose in HCO_3-free Krebs Ringer (KR) buffer containing 139 mM NaCl, 5 mM KCl, 1 mM $MgCl_2$, 2.2 mM $CaCl_2$, 20 mM HEPES and 0.2 % BSA, and pH adjusted to 7.4. Subsequently, the cells were gently washed in KR buffer and allowed to rest for at least 15 min. The cells were mounted in a temperature-regulated chamber (37°C), and all experiments were conducted in a standing-bath configuration. For the Ca^{2+} depletion, the media was changed to nominal Ca^{2+} free KR buffer (139 mM NaCl, 5 mM KCl, 1 mM $MgCl_2$, 20 mM HEPES, 0.2 % BSA and 5mM EGTA) supplemented with 1.67 mM glucose. After 5 to 10 min of Ca^{2+} depletion, 1 μM Thapsigargin was added. For the reintroduction of Ca^{2+}, the cells were gently washed in KR buffer (containing Ca^{2+}) supplemented with 16.67 mM glucose. Finally, the cells were depolarised in 30 mM KCl. Changes in intracellular Ca^{2+} were monitored with a Nikon Eclipse Ti microscope with a 40x NA1.4 objective. Fura-2 loaded cells were excited at 340 nm for 60 msec and at 380 nm for 60 msec at 5 sec intervals using a TILL Polychrome monochromator. Emission was collected at 500 nm by an image-intensifying, charge-coupled device (CCD) camera (Andor X3 897) and digitized by FEI image processing system (Thermo Fisher Scientific). LA Live Acquisition software was used to control the monochromator and the CCD camera. The intracellular Ca^{2+} was presented as the ratio of Fura-2 fluorescence signals recorded at 340/380 nm. For analysis, regions of interest (ROIs) representing single cells were selected based on a combination of 340, 380 and 340/380 images, and the change in the 340/380 ratio of each ROI was used to monitor changes in intracellular Ca^{2+} in individual cells. For every experiment, responses of 38 to 73 cells were used to calculate the average change in the Fura-2 ratio. Cells not responding to KCl were excluded from the analysis. The area under the curve (AUC) was calculated in excel after extracting a dynamic baseline calculated in the software Origin.

Stimulated insulin secretion assays during Calcium depletion and reintroduction
After one week in S7, cells were dissociated for 5 min with TrypLE Select, reseeded on 24-well plates at a density of 500 k per cm^2, and cultured in S7 media for another week. On the day of the experiment, cells were washed twice with Krebs-Ringer bicarbonate (KR) buffer containing 115 mM NaCl, 5 mM KCl, 1 mM $MgCl_2$, 2.2 mM $CaCl_2$, 20 mM HEPES, 24 mM $NaHCO_3$ and 0.2 % BSA (Sigma, Cat# A7906), and pH adjusted to 7.4. All subsequent incubation steps were carried out at 37°C and 5% CO_2. Before Ca^{2+} depletion, the cells were pre-incubated for 1.5 hrs in the fresh KR buffer supplemented with 1.67 mM glucose. For the Ca^{2+} depletion, the media was changed to nominal Ca^{2+} free KR buffer (139 mM NaCl, 5 mM KCl, 1 mM $MgCl_2$, 20 mM HEPES, 0.2 % BSA and 5mM EGTA) supplemented with 1.67 mM glucose. After 5 min of Ca^{2+} depletion, 1 μM Thapsigargin was added and continued to incubate for 25 min. For reintroduction of Ca^{2+}, the cells were incubated in normal KR buffer supplemented with 16.67 mM glucose for 30 min. Finally, the cells were depolarised in KR buffer with 30 mM KCl (totally) and incubated for 30 min. After each step, the medium was collected, and the cells were washed once with KR buffer. Finally, the cells were harvested, immediately transferred to ice, and sonicated (30 s on, 30 s off, 5 cycles) in ddH_2O for total DNA and Insulin content quantifications. The samples for Insulin content quantifications were diluted 2.5 times in 95% ethanol with 0.18 M HCl. All samples were stored at -80°C until analysis in technical duplicates with commercially available ELISA kits for secreted human CPEP and Insulin according to the manufacturer's recommendations (Mercodia, Cat# 10-1141-01 and 10-1132-01).

In Silico transcription factor binding analysis
The Gene Search function of the online tool at http://motifmap.ics.uci.edu [50,51] was employed to search for transcription factor binding sites in the vicinity of the transcriptional start sites of selected MODY transcription factors and membrane potential regulators that we found transcriptionally dysregulated in the $HNF1A^{+/R272C}$ β cells. We reported whether NEUROD, HNF4, HNF1, and PAX4 binding sites were present in 2,000 base pairs upstream and downstream of the transcriptional start site.

siRNA knockdown of HNF4A
Corrected control S7 cells were dissociated to single cells as described above and reverse transfected with 50 nM of two siRNA against HNF4A (ID# S6697 and S6698) or 150 nM negative control siRNA (Thermo Fisher Scientific, Cat# 4392420) using Lipofectamine RNAiMAX (Thermo Fisher Scientific, Cat# 13778030). In brief, in a 24-well format, 2 μl RNAiMAX was premixed with siRNA(s) in 100 μl OptiMEM medium (Thermo Fisher Scientific, Cat# 31985070), and 20-30 minutes later, 350-500 k cells per cm^2 were added in 400 μl S7 medium supplemented with 10 μM Y-27632. 24 hrs after transfection, cells were harvested for transcriptional analyses.

shRNA knockdown of NEUROD1

Lentivirus was generated using HEK 293T cells cultured in a 10 cm dish with 10% fetal bovine serum (Sigma; F4135). The media was switched with 10 mL of fresh new media after seeding for 1 day. Then the HEK 293T cells were transfected with 5 μg of human NEUROD1 shRNA or shRNA Ctrl plasmids (OriGene, TL311201), 6 μg of packaging plasmids (OriGene, TR30037) in 1.5 mL of Opti-MEM (Life Technologies, 31985-070), and 33 μL of TurboFectin Transfection Reagent (OriGene, TF81001) based on the manufacturer's recommendations. The media was switched after 16-18 hours post-transfection. Viral-containing supernatant was collected at 72 hours post-transfection and concentrated using Lenti Concentrator (OriGene, TR30025). The collected lentivirus was tittered using the Lenti-X™ GoStix™ Plus kit (Takara; 631280). Lentiviral transduction occurred after one week in S7 by seeding 1 million dispersed single corrected control cells into a well of a 24-well plate with 3-4 million lentivirus particles and 10 μg/mL polybrene (Merck, TR-1003). The media was switched 16 hours post-transduction. Cells were cultured 5 days after transfection for stimulated insulin secretion assay and RT-qPCR.

QUANTIFICATION AND STATISTICAL ANALYSIS

Statistical analyses were performed with GraphPad Prism (version 7.0 or 8.0, GraphPad Software). Unless otherwise noted, a paired nonparametric test (Wilcoxon matched-pairs signed-rank test) was used to assess significance. For unpaired data or data with an $N < 6$, an unpaired nonparametric test was used (Mann-Whitney test). Asterisks denote p-values as follows: * $p < 0.05$; ** $p < 0.01$; *** $p < 0.001$. Each N represents a biological replicate (mice or independent experiments), typically the average of 3 wells, which were separately determined in technical duplicates. Data figures illustrate the mean with standard deviation and the values of individual biological replicates.